Marine Micropaleontology xxx (xxxx) xxx

Contents lists available at ScienceDirect

Marine Micropaleontology

journal homepage: www.elsevier.com/locate/marmicro

Research paper

Calcareous nannoplankton response to early Eocene warmth, Southwest Pacific Ocean

Claire L. Shepherd [a,*], Denise K. Kulhanek [b], Christopher J. Hollis [a], Hugh E.G. Morgans [a], C. Percy Strong [a], Kristina M. Pascher [a], James C. Zachos [c]

[a] GNS Science, P.O. Box 30368, Lower Hutt 5040, New Zealand
[b] International Ocean Discovery Program, Texas A&M University, 1000 Discovery Drive, College Station, TX 77845, USA
[c] Earth and Planetary Sciences, University of California, Santa Cruz, USA

ARTICLE INFO

Keywords:
Eocene
Southwest Pacific
Campbell Plateau
Lord Howe Rise
Calcareous nannofossil
Paleoecology
Biostratigraphy

ABSTRACT

Episodes of pronounced climatic warming in the early Eocene (56–48 Ma) provide insights into how biological systems might respond to future climate changes. Eocene climate reconstructions for the Southwest (SW) Pacific have proved challenging due to some disparities between geochemical proxy-based estimates for sea temperatures and estimates derived from climate models. Changes in marine phytoplankton populations through the early Eocene provide a means to evaluate model and proxy-based approaches and also reveal how climatic changes affected the ocean ecosystem. This study documents early to middle Eocene calcareous nannofossil assemblages from legacy Deep Sea Drilling Project (DSDP) sites in the SW Pacific. We integrate nannofossil assemblage changes with foraminiferal-based stable isotopes and other microfossil data to provide updated age models for DSDP Sites 207 (Lord Howe Rise) and 277 (Campbell Plateau), and to infer past environmental change through the early to mid-Eocene in the SW Pacific. Although these sites record a short hiatus in the earliest Eocene, deposition resumed by ~54 Ma, prior to the onset of the Early Eocene Climate Optimum (EECO). Both sites show an increase in warm-water taxa from the onset of the EECO until approximately 50.5 Ma. Abundance of warm-water taxa was higher (~23%) at the EECO onset at the more northerly Site 207 and increased only slightly to ~27%, whereas at Site 277 warm-water taxa comprised only ~3% at the EECO onset but increased to ~31% by 50.5 Ma. Cool-water taxa at both sites were present in very sparse numbers (<3%) through much of the EECO and only began to increase in abundance after 50 Ma, concomitant with a decrease in warm-water taxa. These results are similar to other mid-latitude sites in the SW Pacific and Indian Ocean, including mid-Waipara River (Canterbury Basin, New Zealand) and ODP Site 762 (Exmouth Plateau), and indicate assemblages during the EECO are best described as warm temperate. Benthic $\delta^{18}O$ records from both sites show good agreement with nannofossil trends and, despite the possibility of recrystallization at Site 277, sea surface temperatures (SSTs) indicated by planktic foraminifera also imply warm temperate conditions. This suggests that a warm proto-East Australian Current extended to at least 55°S during the EECO, displacing the proto-Tasman Front southward, which migrated northward after termination of the EECO possibly due to expansion of a proto-Ross Sea Gyre.

1. Introduction

The Southwest (SW) Pacific has been the focus of many paleoclimate studies (e.g., Crouch et al., 2003, 2020; Bijl et al., 2009; Hollis et al., 2009, 2012, 2014; Creech et al., 2010; Pancost et al., 2013; Taylor et al., 2013, 2018; Slotnick et al., 2015; Dallanave et al., 2015, 2016; Hines et al., 2017), particularly for the Eocene (56–48 Ma), when Cenozoic global temperatures reached a maximum during the early Eocene Climatic Optimum (EECO; ~53–49 Ma) and atmospheric CO_2 exceeded 800 ppmv (e.g., Zachos et al., 2008; Anagnostou et al., 2016; Hollis et al., 2019). A consequence of this research has been to highlight discrepancies between marine temperature estimates derived from geochemical proxies, and those derived from climate models. Geochemical temperature proxies indicate that SW Pacific sea-surface

* Corresponding author.
E-mail address: c.shepherd@gns.cri.nz (C.L. Shepherd).

https://doi.org/10.1016/j.marmicro.2021.101992
Received 13 May 2020; Received in revised form 9 March 2021; Accepted 18 April 2021
Available online 20 April 2021

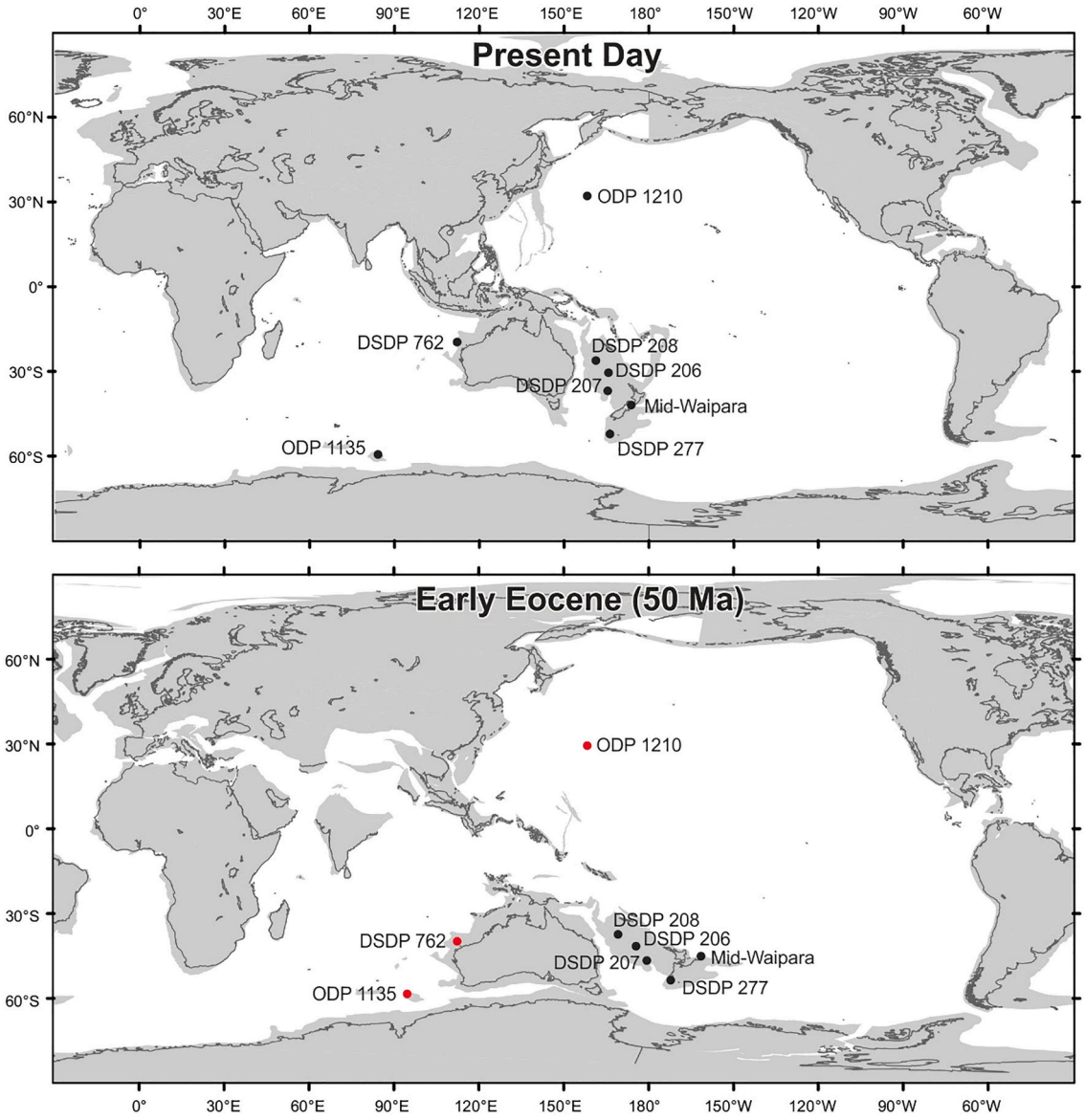

Fig. 1. Location of studied sites and other sites mentioned in the text. Paleogeographic reconstruction at 50 Ma was generated using the relative plate motions of Matthews et al. (2016) and the paleomagnetic reference frame of Torsvik et al. (2012). Red circles indicate an approximated paleolocation at 50 Ma calculated using model version 2.1 of paleolatitude.org, paleomagnetic reference frame Torsvik et al. (2012).

temperatures (SSTs) reached 30 °C or more during the EECO (Bijl et al., 2009; Hollis et al., 2009, 2012, 2019; Creech et al., 2010; Hines et al., 2017; Crouch et al., 2020), implying little to no temperature gradient between low and mid–high latitudes. However, such a low latitudinal temperature gradient has been difficult to reconcile with climate models (Huber and Caballero, 2011; Lunt et al., 2012, 2021).

One way to explore this mismatch between geochemical temperature proxies and climate models is to examine changes within marine phytoplankton assemblages. Studies have demonstrated the efficacy of calcareous nannoplankton biogeography and ecology as indicators of climatic and environmental change (e.g., McIntyre and Bé, 1967; Okada and Honjo, 1973; Haq et al., 1977; Wei and Wise, 1990; Aubry, 1992, 1998; Bralower, 2002; Persico and Villa, 2004; Gibbs et al., 2006; Villa et al., 2008; Kalb and Bralower, 2012; Cappelli et al., 2020; Crouch et al., 2020). Determining the ecological preferences of extinct nannoplankton can be problematic due to the interconnectivity of factors such as temperature and nutrient supply (Agnini et al., 2007b). Additionally, some fossil species are inferred to have undergone an evolutionary shift in their ecological preference over time (Haq and Lohmann, 1976). However, despite these difficulties, there is general agreement that certain species reflect specific environmental conditions such as SST and nutrient conditions (e.g., Wei and Wise, 1990; Wei et al., 1992; Bralower, 2002; Gibbs et al., 2006; Villa et al., 2008, 2014).

These known ecological preferences can be used to reconstruct oceanographic change through time. Comparing changes in assemblages across different latitudes helps to document how nannoplankton responded to changes in SST, productivity and ocean circulation. Here we present analyses of early to middle Eocene calcareous nannofossil assemblages from four legacy Deep Sea Drilling Project (DSDP) sites in the SW Pacific (Fig. 1). We utilize changes in nannofossil assemblages in conjunction with stable isotope analysis and other microfossil data to infer past environmental change through this time interval.

2. Calcareous nannofossil paleoecological indicators

The genus *Chiasmolithus* is largely regarded as having preferred cool-water environments (Bralower, 2002; Persico and Villa, 2004; Villa et al., 2008). Bukry (1973) suggested that during the Eocene this genus

was most abundant at cool-water, high-latitude sites. However, Wei and Wise (1990) suggested that an increase in the abundance of chiasmoliths towards higher latitudes in the middle Eocene–Oligocene only applied to the group as a whole and some larger species, such as *Chiasmolithus gigas* and *C. grandis*, were rare or absent at higher latitudes. Self-Trail et al. (2012) further contended that some species of *Chiasmolithus* go into refugia during periods of warmth (e.g., Paleocene-Eocene Thermal Maximum [PETM]). Aubry (1998) proposed that this group was adapted to mesotrophic or eutrophic environments. Recent work by Cappelli et al. (2020) suggested that some larger forms, such as *C. gigas*, may have been K-mode strategists better adapted to warm and oligotrophic environments. These authors proposed a new genus, *Pletolithus*, to formalize the grouping of taxa that were previously included in the informal *C. gigas* group (e.g., Bown and Newsam, 2017). We adopt this new nomenclature throughout the rest of this paper and *Pletolithus gigas* is not included in the cold-water assemblage for this study.

Coccolithus formosus (= *Ericsonia formosa*) is thought to have preferred warm-water environments (Wei et al., 1992; Villa et al., 2008). A latitudinal transect of the South Atlantic Ocean demonstrated that this species was virtually absent at high latitudes in the middle Eocene–Oligocene but abundant at low to middle latitudes (Wei and Wise, 1990). Furthermore, a decrease in the abundance of *C. formosus* beginning in the middle Eocene (~41.3 Ma) was associated with cooling at that time (Wei and Wise, 1990).

Discoaster is considered to have preferred warm-water, and its abundance generally decreased towards higher latitudes (Bukry, 1973; Wei and Wise, 1990). However, some studies have found that *Discoaster* abundance at some equatorial sites was lower than that in mid-latitudes (Haq and Lohmann, 1976; Wei and Wise, 1990). This suggests that abundance of the genus was affected by other factors in addition to temperature. Aubry (1992) suggested that *Discoaster* was adapted to oligotrophic conditions and the abundance of this group at high latitudes during the early Eocene can be attributed to this factor as much as it can to temperature. Likewise, its decrease in abundance through the late Eocene could be due to the contraction of oligotrophic environments and not solely a response to cooling conditions. Villa et al. (2008) argued that although there was evidence to suggest that *Discoaster* abundance was affected by nutrient supply during the middle Eocene, the reason for its eventual disappearance at Southern Ocean sites in the late middle Eocene was most likely due to a decrease in SST. In this study, we include *Discoaster* as a warm-water indicator in our paleoecological interpretations.

Reticulofenestra daviesii was abundant at high latitude sites but virtually absent or very rare at equatorial sites in the Paleogene (Wei and Wise, 1990; Wei et al., 1992). Given this and that the abundance of *R. daviesii* generally parallels that of the *Chiasmolithus* group, it is therefore regarded as a cool-water indicator (Wei and Wise, 1990; Persico and Villa, 2004; Villa and Persico, 2006). However, the absence of *R. daviesii* from the base of the sections in this study should not be interpreted as an indication of warmer temperatures, as *Reticulofenestra* did not evolve until ~52 Ma in the southern high latitudes and migrated to mid- to low latitudes slightly later (Schneider et al., 2011; Hollis et al., 2015; Shepherd and Kulhanek, 2016).

Sphenolithus is a dominant component of assemblages at equatorial sites but its abundance declines in the mid- to high latitudes. Diversity follows a similar pattern, with high diversity at low latitudes and decreasing diversity in mid- to high latitudes. These factors, combined with its close association with *Discoaster*, are interpreted as a preference for oligotrophic and or warm-water conditions (Wei and Wise, 1990; Bralower, 2002). At some localities, *Sphenolithus* decreased in abundance across the PETM, which is contrary to what is expected, given its preference for warm conditions. Instead, it appears that its low abundance through this interval was driven by high nutrient supply and more eutrophic conditions at sites where this decrease is observed (Gibbs et al., 2006; Agnini et al., 2007b). Other studies also suggest that some species of *Sphenolithus* were able to adapt to mesotrophic or eutrophic conditions. An increase in the relative abundance of *Sphenolithus predistentus* is observed across the Eocene-Oligocene transition and is thought to be associated with an increase in nutrient availability (Dunkley Jones et al., 2008; Fioroni et al., 2015).

3. Paleogeographic setting of the Southwest Pacific in the early–middle Eocene

During the early Eocene the SW Pacific looked very different from today, with Zealandia positioned ~10° further south than its present-day location (Fig. 1). Zealandia had a passive continental margin from the Late Cretaceous to late Paleogene and was relatively tectonically quiescent (Sutherland, 1999). Nelson and Cooke (2001) suggested that during the Eocene, the ocean around New Zealand was bathed in subtropical surface waters fed by the western limb of a South Pacific anticyclonic gyre. Furthermore, prior to the opening of the Tasman gateway, the southward extension of a proto-East Australian Current (EAC) resulted in tropical to warm subtropical water in the south Tasman Sea and New Zealand region (Kennett and Exon, 2004; Sijp et al., 2011). Other authors contend that an Antarctic-derived, northward flowing Tasman Current existed throughout the Paleogene (Bijl et al., 2009, 2011, 2013). Jenkins (1993) documented a transition zone in the Southern Ocean, between warm subtropical and temperate (cool subtropical) waters in the late Paleocene to early Eocene. Nelson and Cooke (2001) inferred that this transition zone was located further south during the early–middle Eocene, based on the presence of warm subtropical to marginally tropical marine biota and relatively high SSTs estimated from oxygen isotopes for that interval.

The southern location of Zealandia during the early Cenozoic affected nannoplankton assemblages. In general, nannoplankton are cosmopolitan but, as noted above, some taxa have specific environmental preferences. As a result, some warm-water taxa show delayed first appearances in the early Paleogene of the SW Pacific relative to other regions. For example, both *Ellipsolithus macellus* and *Sphenolithus primus* cannot be used as biostratigraphic markers for the early Paleocene because they do not appear in the stratigraphic record in New Zealand until the uppermost Paleocene or lower Eocene (e.g., Edwards, 1971; Edwards and Perch-Nielsen, 1974; Kulhanek et al., 2015). Similarly, members of the genus *Rhomboaster* are rare or absent from the New Zealand region (e.g., Edwards, 1971; Edwards and Perch-Nielsen, 1974; Hollis et al., 2015; Shepherd and Kulhanek, 2016). This short-lived genus first appeared at the base of the Eocene, coincident with the Paleocene/Eocene Thermal Maximum (PETM) (uppermost Zone NP9) (Agnini et al., 2007b). *Rhomboaster bramlettei* evolved shortly after (55.86 Ma) and is the marker for the base of Zone NP10. It survived for ~1.5 Myr, disappearing at ~54.42 Ma (Agnini et al., 2007b). This group gave rise to *Tribrachiatus*, including *T. contortus* and *T. orthostylus*. Of these taxa, only *T. orthostylus*, which evolved in latest NP10, is regularly found in SW Pacific assemblages. While this could be used to infer that a significant portion of the earliest Eocene (e.g., most of NP10) is missing from SW Pacific sections, the PETM is recorded at several localities including Tawanui (Crouch et al., 2003), Mead Stream (Hollis et al., 2005a) and DSDP Site 277 (Hollis et al., 2015), none of which contain *Rhomboaster* spp. or *T. contortus*. On the other hand, *R. bramlettei* and *R. cuspis* are found in the lowermost Eocene of the mid-Waipara River section in Canterbury Basin (Shepherd and Kulhanek, 2016). This ambiguity makes identifying the Zone NP9/NP10 boundary in the SW Pacific difficult.

3.1. Lord Howe Rise

DSDP Leg 21 drilled several sites on or near Lord Howe Rise in 1971, including Sites 207 and 208 on Lord Howe Rise, and Site 206 in the adjacent New Caledonia Trough. The cored sediment indicates relatively continuous deposition during the Neogene and Quaternary, but the Paleogene sediments are disrupted by hiatuses (Burns et al., 1973;

Kennett and von der Borch, 1986). We sampled lower to middle Eocene sediments from Site 207, and middle Eocene and Oligocene sediments across a regional late Eocene-early Oligocene unconformity from Sites 206 and 208.

3.1.1. DSDP Site 207

DSDP Site 207 is located on the southern part of the Lord Howe Rise (36° 57.75′S, 165° 26.06′E) at a water depth of 1389 m (Fig. 1). Two holes were continuously cored to a maximum depth of 513 m below the seafloor (mbsf). The upper 309 m of the section comprises Paleocene, early to middle Eocene, early middle Miocene, and late Miocene to late Pleistocene sediments, primarily foraminiferal-nannofossil ooze and chalk, with some siliceous microfossil bearing foraminifer-nannofossil ooze. Upper Cretaceous sediments from 309 to 513 mbsf are comprised mainly of rhyolitic tuffs and vitrophyric rhyolite flows, with ~50 m of glauconitic silty claystone at 309–357 mbsf (Burns et al., 1973). During the early Eocene, Site 207 was situated ~10° further south than its current position, at a paleolatitude of ~46°S (Fig. 1).

3.1.2. DSDP site 208

DSDP Site 208 is also located on the northern part of the Lord Howe Rise (26° 06.61′S, 161° 13.27′E; 1545 m water depth). A single hole was spot cored at this site to a total depth of 594 mbsf, recovering sediments dated to the latest Cretaceous to middle Paleocene, mid-Eocene and late Oligocene to Pleistocene. The sediment is very similar to that collected at Site 207, consisting primarily of foraminiferal-nannofossil ooze, with an increasing abundance of siliceous microfossils in the Paleogene sequences (Burns et al., 1973). Site 208 was also located ~10° further south than present in the Eocene at a paleolatitude of ~36°S (Fig. 1).

3.1.3. DSDP site 206

DSDP Site 206 is located in the New Caledonia Trough (32° 00.75′S, 165° 27.15′E; 3196 m water depth), east of the Lord Howe Rise. Four holes were drilled at Site 206, although only two recovered cores (Holes 206 and 206C). Hole 206 was continuously cored to 416 mbsf. Hole 206C was drilled without coring to 404 mbsf and then spot cored to a total depth of 734 mbsf. The sediment is dated to the Paleocene to early late Eocene and mid-Oligocene to recent and consists primarily of nannofossil ooze and chalk, with variable foraminiferal content. Eocene sediment also contains abundant radiolarians, as well as variable proportions of diatoms and sponge spicules (Burns et al., 1973). Site 206 was located at ~42°S in the Eocene (Fig. 1).

3.2. Campbell Plateau

3.2.1. DSDP Site 277

DSDP Site 277 was drilled in 1973 as part of DSDP Leg 29 and is located on the southern Campbell Plateau between Auckland and Campbell Islands (52° 13.43′S, 166° 11.48′E) at a water depth of 1214 m (Fig. 1). A single hole was drilled and spot cored to a maximum penetration of 472.50 mbsf. Sediments comprise 462 m of middle Paleocene to upper Oligocene nannofossil ooze and chalk, overlain by 10 m of Pliocene–Pleistocene foraminiferal and nannofossil ooze (Shipboard Scientific Party, 1975). Site 277 was located at a paleolatitude of ~54°S during the early Eocene (Fig. 1).

4. Materials and methods

4.1. Samples

This study utilizes 29 samples from DSDP Site 207 (cores 10, 11, 14–26), 8 samples from Site 208 (core 27), and 7 samples from Site 206 (cores 10 and 11) obtained from the Kochi Core Center, Kochi University, Japan. Nineteen samples from Site 277 (cores 36–41) were obtained from the Micropaleontology Reference Centre, GNS Science, New Zealand. Samples analyzed from Sites 207 and 277 span the lower to middle Eocene and samples from Sites 206 and 208 targeted a regional unconformity separating middle Eocene sediments below from Oligocene sediments above. Sampling resolution at all sites was fairly low; on average 5.17 m at Site 206, 5.26 m (~400 kyr/sample) at Site 207, 0.85 m at Site 208, and 2.41 m at Site 277 (~225 kyr/sample). Sampling resolution is much higher across the PETM interval through Zones NP9–10 at Site 277, averaging ~30 kyr/sample.

4.2. Microfossils

4.2.1. Calcareous nannofossils

Smear slides were made using standard techniques (Bown and Young, 1998). In some cases, samples containing a large amount of fine sand were prepared as strewn slides (Bown and Young, 1998). All material is stored in the National Paleontology Collection at GNS Science. Slides were analyzed using an Olympus BX53 microscope at 1000× or 1250× magnification or a Zeiss Axiophot microscope at 1000× magnification (some slides from Site 207) in plane-transmitted light (PL), cross-polarized light (XPL) and phase contrast (PC) light.

Data were collected by counting 450 specimens along random traverses of each slide, followed by further scanning (typically at least 400 fields of view) to identify rare species not recorded in the initial count. Specimens were identified to species level following the taxonomic concepts of Perch-Nielsen (1985), Bown (1998, 2005), Dunkley Jones et al. (2009) and Shamrock and Watkins (2012). Results are correlated to the biostratigraphic zonation scheme of Martini (1971), with subzones as defined by Aubry (1991). Absolute ages for events are based on the 2012 geological time scale (GTS2012; Gradstein et al., 2012; and references therein). The CNE biozones of Agnini et al. (2014) are also noted and are included in figures and tables. Census counts were converted to percentages for paleoecological analysis of the lower to middle Eocene assemblages examined from Sites 207 and 277. All taxa discussed in this paper are listed in the systematic paleontology (Appendix 1) and full synonymies are available in the publications mentioned above. The distribution of calcareous nannofossil taxa is given in Appendix 2.

4.2.2. Foraminifera

Approximately 7–20 g of air-dried sediment from each sample was washed over a 63 μm or 75 μm screen. The residues were then dried, reweighed and half was retained for assemblage analysis. At Sites 206, 208, 277 and the younger interval (143.65–138.55 mbsf) of Site 207, the residue was picked for faunal assemblage analysis utilized solely for biostratigraphy, although census data are available for future analysis (Appendix 3). For the older interval (286–170.19 mbsf) at Site 207, residues were examined for marker taxa only and no census data are available. Taxonomic concepts for the planktic foraminiferal species are those of Jenkins (1971), de Hornibrook et al. (1989), and Pearson et al. (2006). The benthic foraminiferal species concepts follow those of de Hornibrook et al. (1989), van Morkhoven et al. (1986), and Tjalsma and Lohmann (1983). Samples were assigned to New Zealand Stages and their correlative ages (Raine et al., 2015), which are mainly based on GTS2012. All material is stored in the National Paleontology Collection at GNS Science, Lower Hutt, New Zealand.

4.3. Stable isotope analysis

Stable isotope analysis of foraminifera was carried out in the Stable Isotope Laboratory at the University of California, Santa Cruz (Appendix 4). Between 1 and 6 (average of 3) specimens of *Cibicides*, 3–17 (average of 10) specimens of *Acarinina*, 2–10 (average of 4) specimens of *Morozovella*, and 1–8 (average of 5) specimens of *Subbotina* were used in each analysis. Specimens were first sonicated in deionized water to remove clay and detrital calcite. Isotopic measurements were carried out on a Thermo Finnigan MAT253 mass spectrometer interfaced with a Kiel device. The analytical precision (1σ) is based on repeat analysis of an in-

Table 1
Calcareous nannofossil, foraminifera and radiolarian datums for DSDP Sites 207 and 277. Group = Foraminifera, calcareous Nannofossils, Radiolaria; Event = First and Last Occurrence; Zone = base, lower, mid-, top, upper. Radiolarian events are from Pascher (2017) and Hollis et al. (2020).

Taxon	Abbrev.	Group	Event	Zone	Age (Ma)	Reference	Bottom Depth (mbsf)	Top Depth (mbsf)	Midpoint Depth (mbsf)	± (m)
DSDP Site 207										
Reticulofenestra umbilicus (>14 μm)	Rumb	N	FO	lNP16	41.94	Gradstein et al. (2012)	182.00	171.51	176.76	5.25
Globigerinatheka index	Gind	F	FO	bAb	42.60	Raine et al. (2015)	189.40	168.50	178.95	10.45
Eusyringium fistuligerum	Efis	R	FO	bzRP12	42.85	Dallanave et al., 2015	170.19	168.50	169.35	0.84
Pletolithus gigas	Cgig	N	LO	tNP15b	44.12	Gradstein et al. (2012), Agnini et al. (2014)	182.00	171.51	176.76	4.51
Eusyringium lagena	Elag	R	FO	bzRP11	45.24	Dallanave et al. (2015)	189.40	182.00	185.70	3.70
Pletolithus gigas	Cgig	N	FO	bNP15b/ bCNE10	45.49	Gradstein et al. (2012), Agnini et al. (2014)	207.52	198.51	203.02	4.51
Morozovella crater	Mcra	F	LO	bDp	45.70	Raine et al. (2015)	213.40	212.00	212.70	0.70
Discoaster lodoensis	Dlod[G]	N	LO	uNP14b	47.41	Gradstein et al. (2012)	230.01	219.47	224.74	5.27
Nannotetrina cristata	Ncri	N	FO	lNP14b/ bCNE8	47.73	Gradstein et al. (2012), Agnini et al. (2014)	230.01	219.47	224.74	5.27
Discoaster lodoensis	Dlod[A]	N	LO	lNP14/ bCNE7	47.81	Agnini et al. (2014)	230.01	219.47	224.74	5.27
Elphidium hampdenense	Eham	F	FO	bDh	48.90	Raine et al. (2015)	230.01	219.47	224.74	5.27
Discoaster sublodoensis	Dsub	N	FO	bNP14	49.11	Gradstein et al., 2012	247.26	242.46	244.86	2.40
Artobotrys auriculaleporis	Aaur	R	FO	lzRP10	49.70	Dallanave et al. (2015)	245.38	242.46	243.92	1.46
Tribrachiatus orthostylus	Tort	N	LO	bNP13/ bCNE5	50.50	Gradstein et al. (2012), Agnini et al. (2014)	271.50	269.60	270.55	0.95
Buryella tetradica	Btet	R	LO	tzRP9	51.00	Dallanave et al. (2015)	279.00	276.51	277.76	1.25
Morozovella crater	Mcra	F	FO	bDm	52.00	Dallanave et al. (2015), Raine et al. (2015)	279.00	269.00	274.00	3.76
Theocampe urceolus	Turc	R	FO	mzRP9	52.80	Dallanave et al. (2015)	284.20	279.00	281.60	2.60
Lychnocanium bellum	Lbel	R	FO	bZRP9	53.20	Dallanave et al. (2015)	286.00	284.20	285.10	0.90
Discoaster lodoensis	Dlod	N	FO	bNP12	53.70	Gradstein et al. (2012)	279.00	276.51	277.76	1.25
Sphenolithus radians	Srad	N	FO	bNP11	54.17	Gradstein et al. (2012)	286.00	284.20	285.10	0.90
Tribrachiatus orthostylus	Tort	N	FO	uNP10/ bCNE3	54.37	Gradstein et al. (2012), Agnini et al. (2014)	286.00	284.20	285.10	0.90
Fasciculitus spp.	Fasc	N	LO	lNP10	55.64	Gradstein et al. (2012)	286.00	284.20	285.10	0.90
DSDP Site 277										
Reticulofenestra umbilicus (>14 μm)	Rumb	N	FO	lNP16	41.94	Gradstein et al. (2012)	370.58	369.00	369.79	0.79
Morozovella crater	Mcra	F	LO	bDp	45.70	Raine et al. (2015)	380.75	372.08	376.42	4.33
Phormocyrtis striata striata	Pstr	R	LO	ZRP10	47.00	Hollis et al. (2020)	387.95	380.75	384.35	3.60
Discoaster lodoensis	Dlod[G]	N	LO	uNP14b	47.41	Gradstein et al. (2012)	387.95	381.50	384.73	3.23
Nannotetrina cristata	Ncri	N	FO	lNP14b/ CNE8	47.73	Gradstein et al. (2012), Agnini et al. (2014)	372.08	370.58	371.33	0.75
Discoaster lodoensis	Dlod[A]	N	LO	lNP14	47.81	Agnini et al. (2014)	387.95	381.50	384.73	3.23
Amphicraspedum prolixum	Apro	R	LO	ZRP10	48.80	Hollis et al. (2020)	409.33	407.83	408.58	0.75
Discoaster sublodoensis	Dsub	N	FO	bNP14	49.11	Gradstein et al. (2012)	391.00	389.50	390.25	0.75
Artobotrys auriculaleporis	Aaur	R	FO	lZRP10	49.70	Dallanave et al. (2015)	426.34	416.20	421.27	5.07
Tribrachiatus orthostylus	Tort	N	LO	bNP13/ bCNE5	50.50	Gradstein et al. (2012), Agnini et al. (2014)	426.53	419.60	423.07	3.46
Buryella tetradica	Btet	R	LO	tZRP9	51.00	Dallanave et al. (2015)	437.75	436.78	437.27	0.49
Morozovella crater	Mcra	F	FO	bDm	52.00	Dallanave et al. (2015), Raine et al. (2015)	427.12	426.90	427.01	0.11
Artobotrys biaurita	Abia	R	FO	uZRP9	52.50	Hollis et al. (2020)	426.90	416.20	421.55	5.35
Lychnocanium bellum	Lbel	R	FO	bZRP9	53.20	Dallanave et al. (2015)	)409.33	407.83	408.58	0.75
Discoaster lodoensis	Dlod	N	FO	bNP12	53.70	Gradstein et al. (2012)	434.57	429.40	431.99	2.59
Discoaster multiradiatus	Dmul	N	LO	NP11	54.00	Gradstein et al. (2012)	445.15	438.90	442.03	3.13
Lychnocanium auxillum	Laux	R	LO	tZRP8	54.10	Dallanave et al. (2015)	438.71	416.20	427.46	11.26
Sphenolithus radians	Srad	N	FO	bNP11	54.17	Gradstein et al. (2012)	446.92	446.50	446.71	0.21
Tribrachiatus orthostylus	Tort	N	FO	uNP10/ bCNE3	54.37	Gradstein et al. (2012), Agnini et al. (2014)	446.92	446.50	446.71	0.21
Morozovella lensiformis	Mlen	F	FO	mDw	55.00	Cooper (2004)	446.31	445.15	445.73	0.58
Fasciculithus tympaniformis	Ftym	N	LO	lNP10/ bCNE2	55.64	Gradstein et al. (2012), Agnini et al. (2014)	446.92	446.50	446.71	0.21
Amphicraspedum prolixum	Apro	R	FO	bZRP8	55.96	Hollis et al. (2020)	447.71	447.51	447.61	0.10
Podocyrtis papalis	Ppap	R	FO	bZRP8	55.96	Dallanave et al. (2015)	447.71	447.51	447.61	0.10
Phormocyrtis striata striata	Pstri	R	FO	lZRP7	57.20	Hollis et al. (2005a, 2005b)	447.51	447.01	447.26	0.25
Base of PETM onset	bPETM	G	–	–	55.96	Gradstein et al. (2012)	457.30	457.27	457.29	0.02
Discoaster multiradiatus	Dmul	N	FCO	NP9	57.21	Gradstein et al. (2012)	462.43	460.61	461.52	0.91

house standard (Carrara marble), calibrated to the international standards NBS18 and NBS19, and averages ± 0.05‰ for $\delta^{13}C$ and ± 0.08‰ for $\delta^{18}O$. All values are reported relative to VPDB. For the $\delta^{18}O$ values of *Cibicides*, we apply an isotopic correction factor of + 0.28‰ (Katz et al., 2003). Paleotemperatures for both benthic and planktic taxa were estimated from $\delta^{18}O$ using the equation of Kim and O'Neil (1997) as recommended by Hollis et al. (2019). Ice-free conditions are assumed and no correction for latitude has been applied.

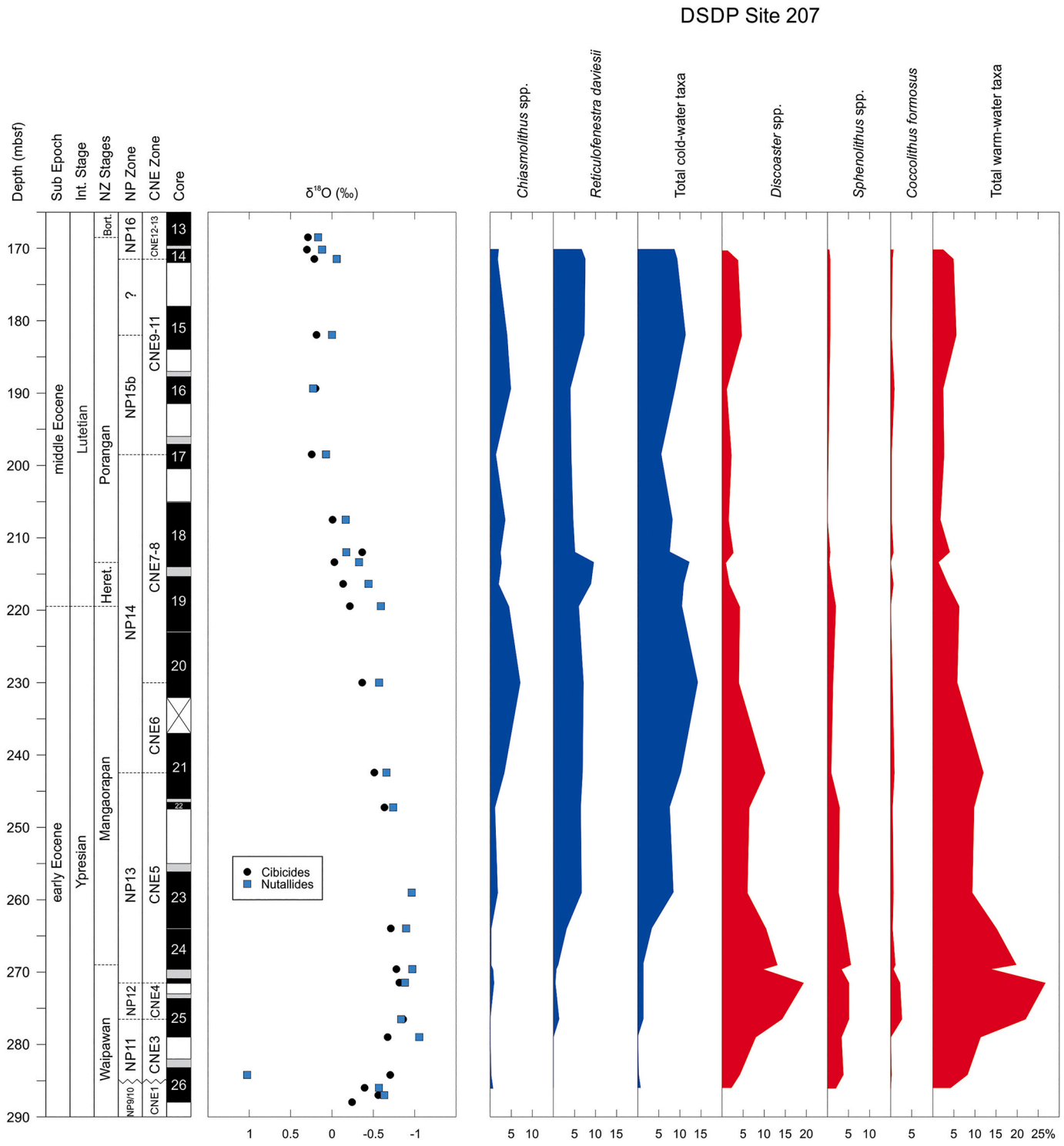

Fig. 2. Oxygen isotope record ($\delta^{18}O$) and relative abundance of nannofossil cool- and warm-taxa from DSDP Site 207, plotted against depth, nannofossil zones and New Zealand Stages. Blue = cool-water taxa, Red = warm-water taxa. NP Zones based on Martini (1971), CN Zones based on Agnini et al. (2014), New Zealand Stages based on Raine et al. (2015), events calibrated to Gradstein et al. (2012).

5. Results

5.1. DSDP Site 207

5.1.1. Calcareous nannofossils

Calcareous nannofossils are common to abundant throughout the studied interval and have variable preservation. Poor to moderate preservation was observed from 286–271.50 mbsf and 198.51–182 mbsf, whereas moderate to good preservation was observed from 269.60–207.52 mbsf. Distribution of calcareous nannofossil taxa is shown in Appendix 2 and biostratigraphic datums are given in Table 1.

Discoaster multiradiatus (first common occurrence [FCO] = 57.21 Ma) is observed in the lowermost sample (286 mbsf), indicating placement within Zone NP9 or younger (Fig. 2). The genus *Fasciculithus*, which ranges from Zone NP4 to early NP10 (Agnini et al., 2014), is also observed in this basal sample. The absence of *Rhomboaster bramlettei*,

whose first occurrence (FO) marks the base of Zone NP10 (55.86 Ma), could restrict the base of the investigated section to Zone NP9. However, given that this lineage is rare or absent in the SW Pacific, we instead use the presence of *Fasciculithus* spp. (last occurrence [LO] = 55.64 Ma) in this sample to assign it to Zone NP9 to lowermost NP10.

A sampling gap of ~1.8 m occurs between this lowermost sample and the overlying one at 284.20 mbsf. The absence of *Tribrachiatus contortus*, whose last occurrence (LO) marks the top of Zone NP10, is consistent with previous studies that report an incomplete or absent *Rhomboaster* lineage in the New Zealand region (Edwards, 1971; Hollis et al., 2015; Shepherd and Kulhanek, 2016). Instead, we use the FO of *Sphenolithus radians* (54.17 Ma) in the sample at 284.20 mbsf as a secondary marker for the base of Zone NP11 (Backman, 1986; Gradstein et al., 2012). *Tribrachiatus orthostylus*, which has its first appearance in the upper part of Zone NP10 (54.37 Ma), co-occurs with the FO of *S. radians*. The interval from 284.20 to 279 mbsf is assigned to Zone NP11. The FOs of *Reticulofenestra minuta*, *Reticulofenestra producta* and *Reticulofenestra samodurovii* are within this zone.

The FO of *Discoaster lodoensis* (53.7 Ma) is observed at 276.51 mbsf, marking the base of Zone NP12. Samples from 276.50–271.50 mbsf are assigned to Zone NP12. Identification of discoasters to species level in this interval is difficult due to overgrowth.

The LO of *T. orthostylus* (50.5 Ma) is observed at 271.50 mbsf and this event marks the top of Zone NP12. The next sample above at 269.90 mbsf is assigned to Zone NP13, which extends to 247.26 mbsf. *Z. bijugatus* subsp. *bijugatus*, is abundant throughout the zone but becomes less abundant towards the top. *Reticulofenestra daviesii*, *R. dictyoda*, *R. minuta*, *R. producta* and *R. samodurovii* are rare to few in the lower part of this zone but become more common towards the top, where *Reticulofenestra circus* makes its first appearance. *Discoaster kuepperi* is common in the lower part of this zone but decreases in abundance in the upper part.

The FO of *Discoaster sublodoensis* is recorded at 242.46 mbsf, defining the base of Zone NP14. The interval from 242.46 to 207.52 mbsf is assigned to Zone NP14. The marker for the base of Subzone NP14b (*Blackites gladius*) is absent from the section; however, *Chiasmolithus expansus* and *Nannotetrina cristata* have first occurrences within Subzone NP14b (Bown and Newsam, 2017) and first occur at 216.40 mbsf and 219.47 mbsf, respectively. *Toweius callosus* is present in low numbers throughout most of the Zone NP14 interval and *Toweius magnicrassus* occurs sporadically, whereas *Reticulofenestra* spp. are common to abundant.

The FO of *Nannotetrina fulgens* (46.29 Ma), which is the marker for the base of Subzone NP15a, is observed above the FO of *Pletolithus gigas* (the marker for the base of Subzone NP15b; Aubry, 1991) at 182 mbsf. The FO of *P. gigas* (45.49 Ma) is observed at 198.51 mbsf. However, it is unclear whether the absence of *N. fulgens* below the FO of *P. gigas* is due to poor preservation or if Subzone NP15a is missing at Site 207. The LO of *P. gigas* (44.12 Ma) is observed at 182 mbsf and defines the top of Subzone NP15b. The interval from 198.51 to 182 mbsf is assigned to Subzone NP15b. *Reticulofenestra circus* is common in the lower part of this subzone and becomes less abundant towards the top. Conversely, *R. daviesii* becomes more abundant towards the top of the subzone. *Discoaster lodoensis* also occurs within this interval in extremely low numbers.

The base of Zone NP16 is defined by the LO of *Blackites gladius*; however, this taxon is often scarce in assemblages and its range extends above the LO of *N. alata/fulgens* and FO of *R. umbilicus* (Wei and Wise Jr., 1989). Instead, some workers use the LO of *Nannotetrina alata/fulgens* to approximate the base of NP16 (Backman, 1986; Expedition 320/321 Scientists, 2010), although this group is also often rare in assemblages. Agnini et al. (2014) noted this difficulty and their zonation instead defines Zone CNE12 from the LO of *P. gigas* to the FCO of *R. umbilicus*, which correlates to Subzone NP15c to lower Zone NP16. We use the consistent presence of *R. umbilicus* from sample 171.51 to 143.55 mbsf to assign this interval to Zone NP16. There is a 10 m sampling gap between sample 182 mbsf (assigned to Subzone NP15b) and sample 171.71 mbsf (assigned to Zone NP16) so it is not possible to determine if Subzone NP15c is missing due to the sampling gap or a hiatus. The presence of *N. fulgens* (LO = 42.87 Ma) in sample 170.19 mbsf may be due to reworking or could indicate diachroneity in the FO of *R. umbilicus* and LO of *N. alata/fulgens* in this region.

The LO of *Nannotetrina* spp. (41.85 Ma) occurs within the interval assigned to Zone NP16 at 143.85 mbsf and the FO of *Reticulofenestra reticulata* (41.66 Ma) is found in the overlying sample at 143.65 Ma.

A major hiatus is observed between 143.55 and 139 mbsf. The sediment overlying the hiatus is significantly younger (middle Miocene) and is assigned to combined Zone NN4–5 based on the presence of *Sphenolithus heteromorphus*. The FO of this species is near the base of Zone NN4 (17.71 Ma) and its LO marks the top of Zone NN5 (13.53 Ma). The zonal marker for the NN4/NN5 boundary (*Helicosphaera ampliaperta*) is absent from the SW Pacific region (Lohman, 1986), making it difficult to distinguish these zones. The Miocene assemblage is dominated by reticulofenestrids, and common taxa include *C. pelagicus* and *Cyclicargolithus floridanus*. Other taxa that confirm a Miocene age for this section are *Calcidiscus leptoporus*, *C. premacintyrei*, *C. tropicus*, *Cryptococcolithus mediaperforatus*, *Discoaster petaliformis* and *Umbilicosphaera rotula*.

5.1.2. Foraminifera

Four early–middle Eocene New Zealand Stage boundaries are identified at Site 207 using foraminiferal bioevents (Fig. 2). The FO of the planktic foraminifera *Morozovella crater* is observed at 269 mbsf and defines the early Eocene Waipawan/Mangaorapan boundary (52 Ma). A related and possibly early form of this species is observed at 276.51 mbsf. The FO of the benthic foraminifera *Elphidium hampdenense* is identified at 219.47 mbsf, marking the Mangaorapan/Heretaungan boundary (48.9 Ma; early Eocene). The primary datum for the Heretaungan/Porangan boundary (45.7 Ma; middle Eocene), the FO of the benthic foraminifera *Elphidium saginatum*, is not recorded at Site 207. Instead, the LO of *M. crater* at 213.40 mbsf is used as a secondary datum. The consistent FO of *Globigerinatheka index* at 168.50 mbsf marks the Porangan/Bortonian boundary (42.6 Ma; middle Eocene). Two isolated occurrences of this species are observed at 182 mbsf. The interval from 143.54 to 143.55 mbsf also contains a Bortonian assemblage that includes *G. index*, *Acarinina primitiva*, *Acarinina collactea*, and *Acarinina bulbrooki*. Samples from 138.55–139 mbsf contain a completely different planktic foraminiferal assemblage that includes a sinistral population of *Globorotalia miotumida*, *Fohsella peripheroronda*, and robust specimens of *Orbulina suturalis*, which are definitive for the lower Lillburnian Stage (15.1–14.5 Ma; middle Miocene), consistent with nannofossil biostratigraphic results. Therefore, a major unconformity that spans ~20 million years from the late Eocene to the middle Miocene is inferred to occur between 145.55 and 139 mbsf.

5.1.3. Oxygen Isotopes

At Site 207, oxygen isotope ($\delta^{18}O$) measurements of benthic foraminifera show good agreement between the two genera, with overall values ranging from 0.31 to −0.86‰ for *Cibicides*, and 0.23 to −1.05‰ for *Nuttalides* (Fig. 2; Appendix 4). At the base of the studied interval (288–287.02 mbsf; early Eocene), $\delta^{18}O$ for both groups ranges from −0.24 to −0.63‰. A negative shift in $\delta^{18}O$ occurs from 284.22 mbsf, with values for *Nuttalides* reaching −1.05‰ at 279 mbsf and *Cibicides* reaching −0.86‰ at 276.53 mbsf. A gradual positive shift in $\delta^{18}O$ for both groups starts at 247.28 mbsf and continues to the top of the studied interval (168.52 mbsf; middle Eocene), with *Cibicides* values reaching a maximum of 0.31‰ at 170.21 mbsf.

5.1.4. Paleoecology

At Site 207, warm-water taxa (*Discoaster* spp., *Sphenolithus* spp. and *C. formosus*) increase in abundance through Zone NP9–10 to lower Zone NP13 (284.20–269 mbsf; late Paleocene to early Eocene), reaching a

maximum of 26.67% in Zone NP12 (271.50 mbsf; Fig. 2). This increase in warm-water taxa corresponds with a rise in the abundance of all three warm-water indicators; however, *Discoaster* spp. accounts for ~19.3% of the warm-water assemblage at their maximum peak. Cool-water taxa (*Chiasmolithus* spp. and *Reticulofenestra daviesii*) occur in low numbers, reaching no more than 3.3% of the assemblage in this lower part of the section.

From Zone NP13 to upper Zone NP14 (264–213.40 mbsf; early Eocene to middle Eocene), the abundance of cool-water taxa increases steadily, reaching a maximum of 14.2% in lower Zone NP14 (230.01 mbsf). *Reticulofenestra daviesii* increases in abundance in Zone NP13 (264 mbsf), reaching a peak of 9.6% in upper Zone NP14 (213.40 mbsf). *Chiasmolithus* begins to increase in abundance in lower Zone NP14 (242.46 mbsf), attaining a maximum of 7.1% at 230.01 mbsf, and then the abundance declines in the uppermost part of Zone NP14 (216.40–212 mbsf). Warm-water taxa decrease in abundance through this interval, dropping to a low of 1.33% in upper Zone NP14 (213.40 mbsf). This decline is reflected in all three warm-water indicators (Fig. 2).

From upper Zone NP14 to Zone NP16 (212–170.19 mbsf; middle Eocene) the abundance of warm-water taxa remains low, no more than 5.6% of the assemblage. Cool-water taxa decrease slightly in abundance in Subzone NP15b (198.51 mbsf) but increase again in Zone NP16 (189.40–170.19 mbsf) where they make up 8.9–11.3% of the assemblage.

5.2. DSDP Site 206

5.2.1. Calcareous nannofossils

Calcareous nannofossils from Hole 206C are moderately preserved, with slightly poorer preservation in the lower interval (Appendix 2). In the lowest sample examined (649.60 mbsf), the presence of *Reticulofenestra umbilicus* (FO at 41.94 Ma) and absence of *Nannotetrina* spp. (LO at 41.85 Ma) and *Reticulofenestra reticulata* (FO at 41.66 Ma) indicate assignment to Zone NP16, ~41.85–41.66 Ma. The presence of *R. reticulata*, *R. bisecta* > 10 μm (FO at 38.25 Ma), and *C. grandis* (LO at 37.98 Ma) in the overlying sample at 630.13 mbsf indicates upper Zone NP17, ~38.25–37.98 Ma (latest middle Eocene). This zone persists to 613.75 mbsf. A distinct assemblage change in the overlying sample indicates that there is an unconformity between 613.75 and 613.70 mbsf.

The assemblage at 613.70 mbsf is characterized by the presence of *R. bisecta*, *Chiasmolithus altus*, and *Sphenolithus predistentus*, and the absence of *Coccolithus formosus*, *R. reticulata*, *R. umbilicus* and *S. distentus*. A few specimens of older taxa are also present and considered reworked, including *P. gigas* and *Neococcolithes dubius*. The age range is bracketed by the LO of *Reticulofenestra umbilicus*, which is at 31.35 Ma in southern high latitudes (Persico and Villa, 2004; Wei, 2004; Gradstein et al., 2012) and the FO of *Sphenolithus distentus* (30 Ma). This indicates that the sediment overlying the unconformity is within Zone NP23 (early Oligocene) and between 30 and 31.35 Ma in age. This zone continues to the top of the examined section at 613.40 mbsf.

5.2.2. Foraminifera

The five lowest samples (649.60–613.70 mbsf) examined contain a planktic assemblage that includes the index species *G. index* (42.64–34.61 Ma), *A. primitiva* (LO at 39.12 Ma), *A. collactea* (LO at 37.96 Ma), and *A. bullbrooki* (LO at 40.49 Ma); the latter species is restricted to a single sample at 630.13 mbsf (Appendix 3). These species constrain the age of the interval to the late middle Eocene (Bortonian; 42.64–39.12 Ma). Other planktic foraminifera in the assemblage include *Globorotalia cerroazulensis, Subbotina linaperta, Zeauvigerina parri,* and *Zeauvigerina zelandica*. A key benthic species, *Bulimina bortonica,* was also recovered from this interval and supports correlation with the Bortonian. This indicates a slightly older age than the nannofossil biostratigraphy. The foraminifera assemblage indicates that the sample at 613.70 mbsf lies below the unconformity, whereas the nannofossil assemblage from that sample mostly consists of younger taxa with a few Eocene taxa considered reworked, suggesting that the sample taken at 613.70 mbsf spans the unconformity.

There is a significantly different planktic foraminiferal assemblage in samples at 613.55 mbsf, 613.40 mbsf, and 613.25 mbsf. The presence of *Subbotina angiporoides* (LO at 29.84 Ma), *Catapsydrax dissimilis* (late early Whaingaroan), *Globigerina euapertura* (early Whaingaroan to mid-Waitakian), and *Paragloborotalia pseudocontinuosa* (latest early Whaingaroan to Miocene) and the absence of *G. index* (LO at 34.61 Ma) places this interval in the early Oligocene (late early Whaingaroan, 34.6–29.8 Ma) and is consistent with calcareous nannofossil biostratigraphy.

5.3. DSDP Site 208

5.3.1. Calcareous nannofossils

Calcareous nannofossils in Hole 208 are moderately to moderately well preserved, with preservation generally much better than at Site 206. Distribution of calcareous nannofossils is given in Appendix 2. The two lowest samples examined, at 491.33 mbsf and 489.81 mbsf, contain *P. gigas*, indicating placement in Subzone NP15b (middle Eocene). The overlying sample, at 488.30 mbsf contains rare *R. umbilicus* > 14 μm (FO at 41.94 Ma) with rare specimens of *Nannotetrina* spp. (LO at 41.85 Ma), indicating placement in Zone NP16. We cannot identify Subzone NP15c but it could be present in the 1.51 m sampling gap or there could be a small unconformity in the section. The sample at 487.95 mbsf can also be assigned to Zone NP16 based on the presence of *R. umbilicus* and absence of *R. reticulata* (FO at 41.66 Ma). Unlike the underlying sample, *Nannotetrina* spp. are absent from this assemblage, which could suggest a slightly younger age (between ~41.85 and 41.66 Ma) than the sample below.

There is a distinct assemblage change at 487.70 mbsf, indicating a hiatus between 487.95 and 487.70 mbsf. The sample above the hiatus is characterized by the presence of *R. bisecta* > 10 μm, *C. altus*, and *S. distentus*, as well as the absence of *R. umbilicus*. The presence of *S. distentus* (FO at 30 Ma) and absence of *Sphenolithus ciperoensis* (FO at 29.62 Ma) indicate assignment to upper Zone NP23 (early Oligocene). The presence of *S. ciperoensis* at 485.90 mbsf marks the base of Zone NP24, which spans the early/late Oligocene boundary and the continued co-occurrence of *S. ciperoensis* and *S. predistentus* in the uppermost sample examined (485.35 mbsf) indicates that the top of the studied interval is near the early/late Oligocene boundary, albeit still within Zone NP24.

5.3.2. Foraminifera

Planktic foraminifera in Hole 208 are moderately well preserved, although there are a small to moderate number of broken specimens (Appendix 3). The five lowest samples examined (492.80–487.95 mbsf) all contain *Elphidium saginatum*, a key benthic foraminiferal taxon for the New Zealand Porangan Stage (45.7–42.64 Ma). This correlation is supported by the presence of planktic index species *A. primitiva* (LO at 39.12 Ma) and *A. bullbrooki* (LO at 40.49 Ma) and the absence of the Bortonian index species *G. index* (42.64–34.61 Ma). An anomalous occurrence of 7 specimens of *M. crater* in a sample within this interval (489.81 mbsf) may be due to reworking. This species is a key marker for the New Zealand Mangaorapan and Heretaungan stages (53.7–45.7 Ma) with its LO marking the base of the Porangan Stage.

There is a marked faunal change at 487.70 mbsf, with significantly different planktic and benthic assemblages. The presence of *G. euapertura, C. dissimilis, Paragloborotalia pseudocontinuosa, Paragloborotalia nana, Chiloguembelina cubensis, Chiloguembelina ototara*, and abundant *Globorotaloides* spp. and the absence of *Subbotina angiporoides*, whose LO at 29.84 Ma marks the top of the lower Whaingaroan Stage, and *Globoquadrina dehiscens*, whose FO marks the base of the Waitakian Stage (25.2 Ma), place this sample in the late Whaingaroan to Duntroonian Stages. Based on the overall assemblage, it is likely that the five upper samples examined (487.70–485.35 mbsf) are restricted to the late

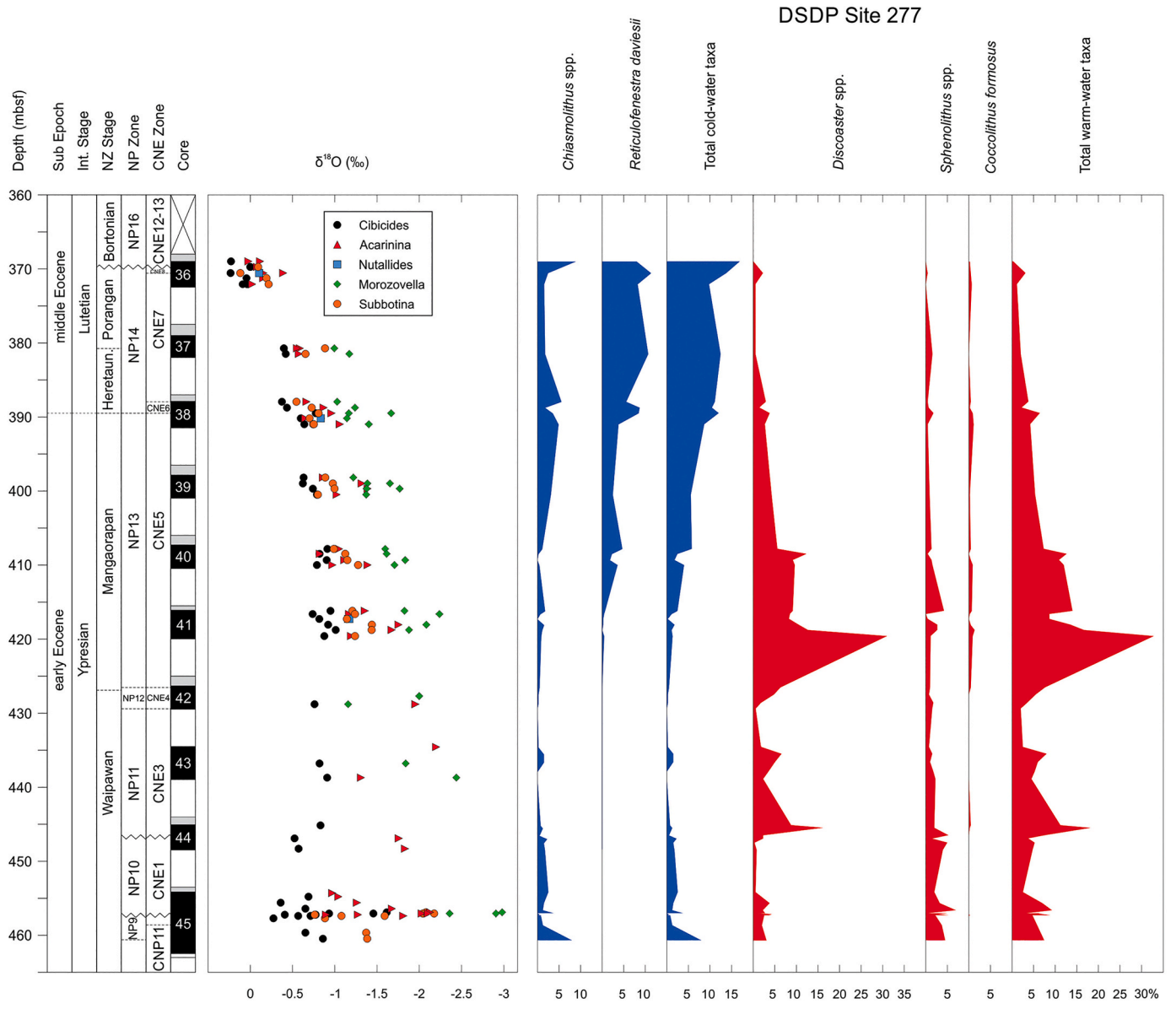

Fig. 3. Oxygen isotope record ($\delta^{18}O$) and relative abundance of nannofossil cool- and warm-taxa from DSDP Site 277, plotted against depth, nannofossil zones and New Zealand Stages. Blue = cool-water taxa, Red = warm-water taxa. NP Zones based on Martini (1971), CN Zones based on Agnini et al. (2014), New Zealand Stages based on Raine et al. (2015), events calibrated to Gradstein et al. (2012).

Whaingaroan (29.84–27.3 Ma), consistent with nannofossil biostratigraphy.

5.4. DSDP Site 277

5.4.1. Calcareous nannofossils

Calcareous nannofossils are common to abundant through the studied interval and show poor to moderate preservation. Distribution of calcareous nannofossil taxa is shown in Appendix 2 and biostratigraphic datums are given in Table 1. In addition to data collected in the current study, we also include count data for the lower interval of this section (460.61–426.53 mbsf). Qualitative data for this interval were published in Hollis et al. (2015).

Discoaster multiradiatus (FCO = 57.21 Ma) is common in the first sample examined at 460.61 mbsf, indicating that the base of the studied section is in Zone NP9 (Fig. 3). The PETM is present between 457.30 and 456.95 mbsf based on the $\delta^{13}C$ record (Hollis et al., 2015), which we use to infer that the interval from 460.61 to 456.98 mbsf (uppermost sample examined within the $\delta^{13}C$ excursion interval) is Zone NP9. Zone NP9 corresponds to upper Zone CNP11 and lower Zone CNE1 (Agnini et al., 2014). The LO of the *Fasciculithus richardii* gr. is found at 458.60 mbsf, marking the top of Zone CNP11.

As noted above, the base of Zone NP10 is defined by the FO of *R. bramlettei*, which occurs shortly after (~100 kyr) the onset of the PETM (Aubry et al., 2007; Gradstein et al., 2012). Since no members of *Rhomboaster* are present at Site 277, we instead use the $\delta^{13}C$ record to infer that the sediment above the PETM $\delta^{13}C$ excursion can be correlated to Zone NP10. At Site 277, the PETM is truncated, with only the first ~66 kyr of the event preserved (Hollis et al., 2015; the full duration is estimated at 170 kyr [Röhl et al., 2007]). The abrupt decrease in *Fasciculithus* spp. and increase in *Zygrhablithus bijugatus* subsp. *bijugatus* at 456.92 mbsf, immediately above the PETM also support the presence of a hiatus between 456.98 and 456.92 mbsf and the Zone NP10 assignment.

Based on the presence of *Fasciculithus* spp. (LO at 55.64 Ma within NP10) from 456.92 to 446.92 mbsf, this interval is assigned to lower

Zone NP10 despite the absence of *Rhomboaster*. The LO of *F. tympaniformis* at 446.92 mbsf also allows this interval to be assigned to Zone CNE1. The next sample (446.50 mbsf) contains both *T. orthostylus* (FO at 54.37 Ma in uppermost NP10) and *S. radians* (FO at 54.17 Ma). We use the latter as a secondary marker for the base of Zone NP11. The co-occurrence of *T. orthostylus* and *S. radians* in this sample suggests that there is a hiatus between 446.92 and 446.50 mbsf. This hiatus could be of short duration, as there is only a 200 kyr difference in age between these two events. However, the presence of *Fasciculithus* spp. (LO 55.64 Ma) at 446.92 mbsf strongly supports that some of Zone NP10 is missing at Site 277. The interval assigned to lower Zone NP10 is correlated to Zone CNE1 (Agnini et al., 2014). Zone CNE2 (duration ~1 Myr) is a gap zone between the LO of *F. tympaniformis* and the FO of *T. orthostylus*, so this zone is missing at Site 277 (or falls within the 40-cm gap between samples).

The interval from 446.50 to 434.57 mbsf is assigned to Zone NP11, extending from the FO of *S. radians* to the FO of *D. lodoensis*, which marks the base of Zone NP12. The NP11 assemblage contains abundant *T. callosus* and common *Z. bijugatus* subsp. *bijugatus*. *Reticulofenestra* spp. first occur in low numbers towards the middle of this zone. This interval is correlative to Zone CNE3.

The FO of *D. lodoensis* (53.7 Ma) is observed at 429.40 mbsf, indicating the base of Zone NP12, and the LO of *T. orthostylus* occurs at 426.53, which marks the top of Zone NP12. The interval from 429.40 to 426.53 mbsf is assigned to Zone NP12. *T. callosus* and *Z. bijugatus* subsp. *bijugatus* are common to abundant in this zone, whereas *Reticulofenestra* spp. remain rare. *Discoaster kuepperi* is rare at the base of this zone but becomes common towards the top. Agnini et al. (2014) use the base of common *D. lodoensis* to define the base of Zone CNE4 (at approximately the same position as the base of Zone NP12), although *D. lodoensis* is only present in rare numbers through Zone NP12 at Site 277, and only becomes common above the LO of *T. orthostylus* (within Zone NP13), which is used to mark the NP12/13 and CNE4/5 zone boundaries.

Zone NP13 extends from 419.60 mbsf (sample above the LO of T. *orthostylus*) to 391 mbsf. *D. kuepperi* becomes rare towards the top of the zone. As at Site 207, *Reticulofenestra* spp. are rare in the lower part of this zone but become more abundant towards the top. The FOs of *R. circus*, *R. producta* and *R. scrippsae* are in the middle to upper part of Zone NP13. This interval correlates to Zone CNE5, which is defined from the LO of *T. orthostylus* to the FCO of *D. sublodoensis*.

The FO of *D. sublodoensis* (49.11 Ma) occurs at 389.50 mbsf and marks the base of Zone NP14; this event provides a secondary datum for the approximate position of the New Zealand Mangaorapan/Heretaungan Stage boundary (48.9 Ma; latest early Eocene; Raine et al., 2015). The LO of *D. lodoensis* and FO of *N. cristata* are datums within Zone NP14 (base of CNE7 and CNE8, respectively [Agnini et al., 2014]). At Site 277, the LO of *D. lodoensis* is observed at 387.95 mbsf and the FO of *N. cristata* is observed at 370.58 mbsf. The interval from 389.50 to 370.58 mbsf is assigned to Zone NP14. *Reticulofenestra* spp. become the dominant member of the assemblage within this zone. *Zygrhablithus bijugatus* subsp. *bijugatus* is common in the lower to middle part of this zone but becomes less abundant towards the top. Both *D. kuepperi* and *S. radians* have last occurrences within Zone NP14.

The absence of *N. fulgens* and *P. gigas* suggests that some, if not all, of Zone NP15 is missing at Site 277. The marker for the base of Zone NP16 (*N. alata/fulgens*) is also absent at Site 277. Instead, the presence of *R. umbilicus* (>14 μm) in the sample at 369 mbsf is used to correlate the top of the studied interval to Zone NP16.

5.4.2. Foraminifera

Three early–middle Eocene New Zealand Stage boundaries are identified at Site 277 using foraminiferal and nannofossil bioevents. The FO of *M. crater* is observed at 426.90 mbsf and is used to define the Waipawan/Mangaorapan boundary (52 Ma; late early Eocene). The FO of the benthic foraminifera *E. hampdenense* is not found at Site 277 and instead, the FO of the nannofossil *Discoaster sublodoensis* at 389.50 mbsf is used as a secondary datum for the Mangoarapan/Heretaungan boundary (48.9 Ma; early Eocene). The FO of the benthic foraminifera *E. saginatum*, is also absent at Site 277 and so the LO of *M. crater* at 380.75 mbsf is used as a secondary datum for the Heretaungan/Porangan boundary (45.7 Ma; middle Eocene). The FO of *G. index* defines the Porangan/Bortonian boundary (42.6 Ma; middle Eocene); however, this event is difficult to identify at Site 277 due to patchy distribution.

5.4.3. Oxygen Isotopes

At Site 277, $\delta^{18}O$ values derived from planktic foraminifera (*Acarinina*, *Morozovella* and *Subbotina*) show some variability between the three genera (Fig. 3; Appendix 4). Values from 448.30–427.71 mbsf (early Eocene) are broadly similar for *Acarinina* and *Morozovella*, ranging from −1.31 to −2.20‰ and −1.16 to −2.44‰, respectively. Values for *Subbotina* were not obtained for this lower interval. A gradual positive shift in $\delta^{18}O$ occurs from 419.60 to 380.75 mbsf (early Eocene to middle Eocene) for all three groups, but the values for *Morozovella* (−1 to −2.24‰) are lower than for *Acarinina* (−0.55 to −1.75‰) and *Subbotina* (−0.55 to −1.44‰). Another positive shift occurs at the top of the studied interval from 372.08–369 mbsf (middle Eocene), with values for *Acarinina* and *Subbotina* ranging from 0.12 to −0.39‰.

The $\delta^{18}O$ values derived from benthic foraminifera (primarily *Cibicides* with a few data points measured on *Nuttalides*) show the same general trend as planktic $\delta^{18}O$ but with some subtle differences. Unlike the planktic record, which has consistent values throughout the interval from 448.30–427.71 mbsf (early Eocene), benthic $\delta^{18}O$ values at the base of the studied interval (448.30–446.92 mbsf; early Eocene) are more positive (−0.52 to −0.57‰) than those obtained from overlying samples. A negative shift occurs from 445.15 to 407.83 mbsf (early Eocene), with values ranging from −0.74 to −1.01‰. A gradual positive shift in $\delta^{18}O$ occurs from 400.50 to 380.75 mbsf (early Eocene to middle Eocene) and values range from −0.37 to −0.79‰. As seen in the planktic $\delta^{18}O$ record, another positive shift occurs at the top of the section from 372.08–369 mbsf (middle Eocene), with values ranging from 0.23 to 0‰. The trends seen in benthic and planktic $\delta^{18}O$ records in this study are consistent with those documented by Shackleton and Kennett (1975).

5.4.4. Paleoecology

At Site 277, the abundance of warm-water taxa (*Discoaster* spp., *Sphenolithus* spp., and *Coccolithus formosus*) are <10% of the assemblage from the base of the studied interval through Zone NP9, reaching a maximum of 8.8% during the PETM. The abundance of cold-water taxa (*Chiasmolithus* spp.) are highest at the base of the studied interval (8%) but decline rapidly within the PETM.

The abundance of warm-water taxa remains at <10% of the assemblage from Zone NP10 (above the PETM) to upper Zone NP12 (448.45–427.50 mbsf; early Eocene), except for a pulse in lower Zone NP11 (445.50–445.15 mbsf) where their abundance reaches 18.25% (Fig. 3). This peak in warm-water taxa is mainly due to a higher abundance of *Discoaster* spp. (16%). The abundance of cold-water taxa (*Chiasmolithus* spp. and *Reticulofenestra daviesii*) remains low through this interval, not reaching more than 2.2% of the assemblage.

The abundance of warm-water taxa starts to increase in upper Zone NP12 (427.50 mbsf) with *Discoaster* spp. abundance increasing to 30.9% at 419.60 mbsf. Above this peak, the abundance of warm-water taxa declines but then remains at fairly constant values (~8.6–14%) throughout lower Zone NP13 (408.50 mbsf; early Eocene). The abundance of cool-water taxa remains low through this interval, at less than 5% of the total assemblage.

Cool-water taxa increase in abundance from upper Zone NP13 (407.83 mbsf; early Eocene), peaking at 16.9% in Zone NP16 (369 mbsf; middle Eocene). As at Site 207 (Fig. 2), the abundance of *Chiasmolithus* spp. decreases in the upper part of the section but the abundance of *R. daviesii* increases. Warm-water taxa continue to decrease in abundance from the middle of Zone NP13 (407.83 mbsf), dropping to less

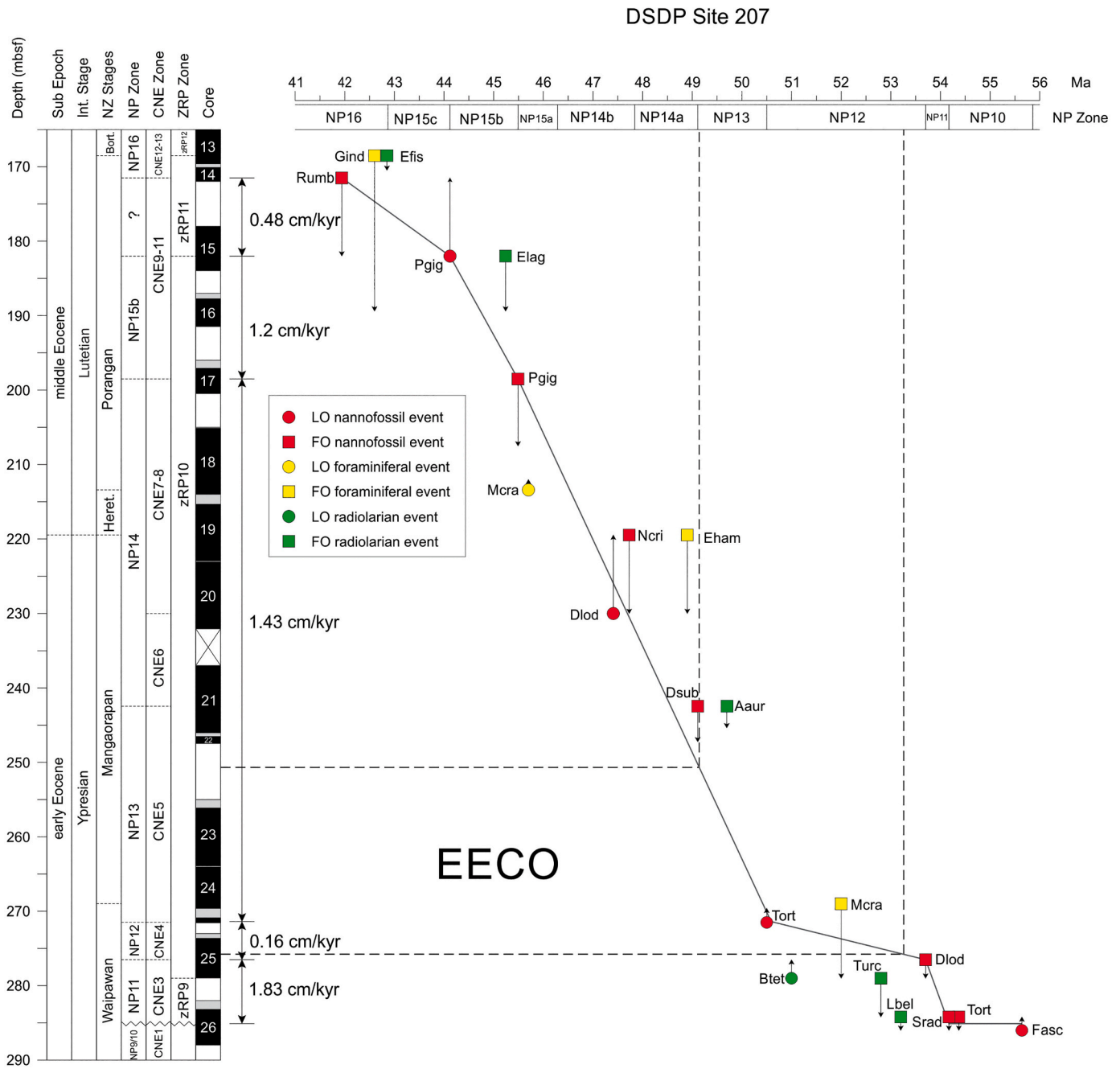

Fig. 4. Age-depth plot for DSDP Site 207. Vertical lines represent the uncertainty between bounding samples and arrows indicate the direction in which the event could move (see text for explanation). The line of correlation represents intervals of constant sediment accumulation rate (SAR) and hiatuses. New Zealand (NZ) Stages are based on bioevents in Raine et al. (2015). Taxa abbreviations shown in Table 1. Black shading represents recovered core, gray shading represents no core recovery and crosses represent core gaps.

than 1% in Zone NP16. This is reflected in the low abundance of all three warm-water indicators.

5.5. Age Models

We used biostratigraphic datums from DSDP Sites 207 and 277 to construct age-depth plots (Figs. 4 & 5) using the following conditions: i) compacted sediment accumulation rate (SAR) is assumed to be relatively constant where lithology is uniform; ii) the line of correlation should lie on or above LOs and on or below FOs; and iii) hiatuses are inferred based on biostratigraphic evidence and where applicable, the clustering of bioevents. The second condition assumes that events are isochronous. Diachronous events are indicated if LOs lie above the correlation line or FOs lie below the line. In addition to the nannofossil and foraminiferal events outlined in the preceding sections, radiolarian datums were incorporated into these age models to improve their robustness. These datums are documented in a companion study of radiolarians at Sites 207 and 277, as part of a regional biostratigraphic review (Hollis et al., 2020). The low resolution of sampling at these sites may have some impact on the strength of these models.

5.5.1. DSDP Site 207

DSDP Site 207 SARs ranged from ~0.16–1.83 cm/kyr through the early to middle Eocene (Fig. 4). A possible hiatus that spans from Zone

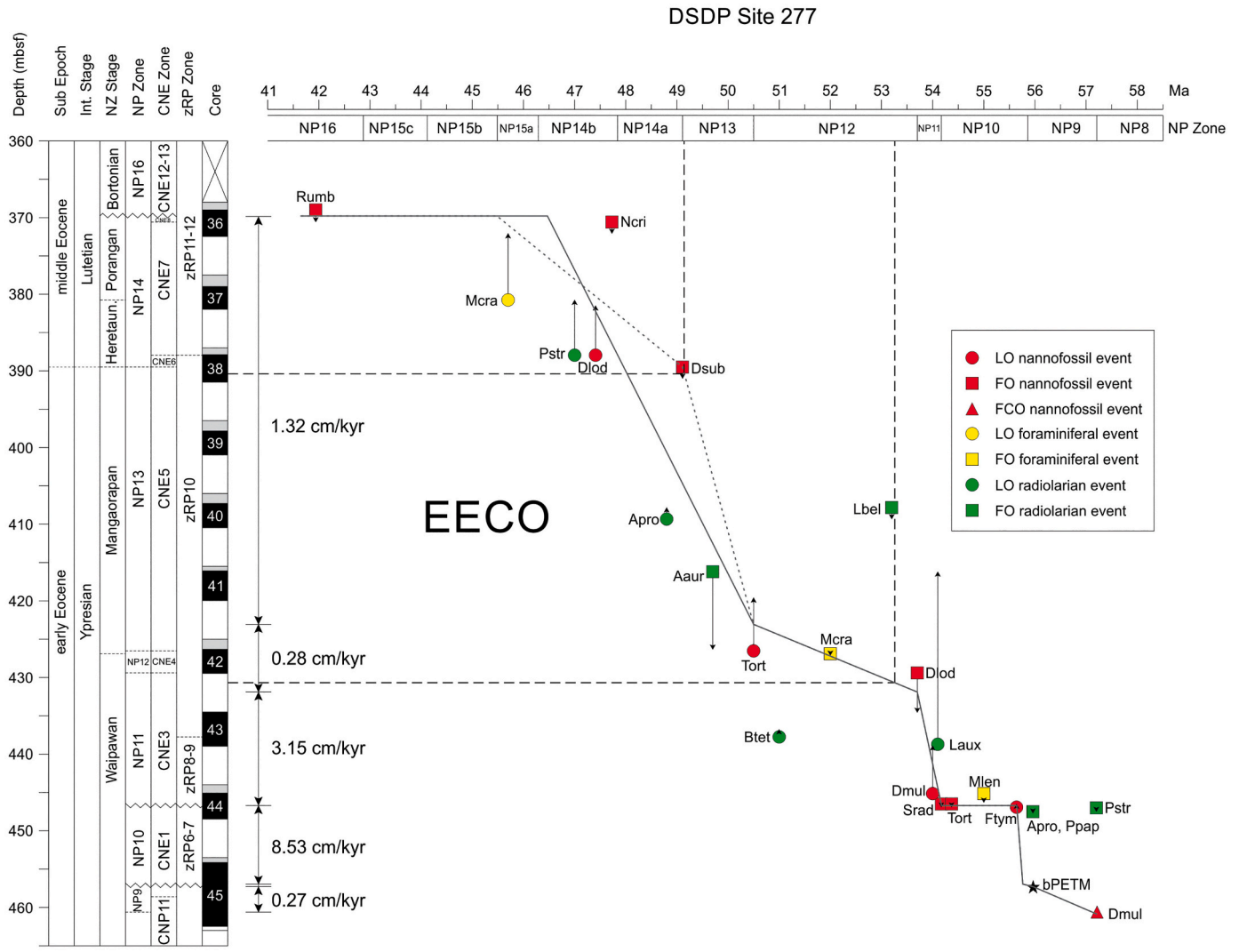

Fig. 5. Age-depth plot for DSDP Site 277. Vertical lines represent the uncertainty between bounding samples and arrows indicate the direction in which the event could move (see text for explanation). The line of correlation represents intervals of constant sediment accumulation rate (SAR) and hiatuses. New Zealand (NZ) Stages are based on bioevents in Raine et al. (2015). Taxa abbreviations shown in Table 1. Black shading represents recovered core, gray shading represents no core recovery and crosses represent core gaps. Dashed line represents an alternative line of correlation.

NP9/10 to lower Zone NP11 is identified at 285 mbsf, based on the clustering of three bioevents (LO of *Fasciculithus* spp., and the FOs of *T. orthostylus* and *S. radians*), although we note that there is a 1.8 m sampling gap between the LOs and FOs. Following this possible hiatus, SARs were 1.83 cm/kyr from 54.17 to 53.7 Ma (285.10–276.51 mbsf), before decreasing to 0.16 cm/kyr from 53.7 to 50.58 Ma (276.51–271.39 mbsf). Recent work from IODP Site U1510, located ~105 km northwest of Site 207 (Fig. 1), documents a comparable linear sedimentation rate (LSR) of 2 m/Myr from 54 to 48 Ma (Sutherland et al., 2019). SARs at Site 207 increased to 1.43 cm/kyr from 50.58 to 45.49 Ma (271.39–198.51 mbsf) and decreased slightly to 1.2 cm/kyr from 45.49 to 44.12 Ma (198.51–182 mbsf). SARs at the top of the studied interval decreased to 0.48 cm/kyr from 44.12 to 41.94 Ma (182–171.51 mbsf).

5.5.2. *DSDP Site 277*

Our age model at Site 277 focuses on the interval above the PETM, as a detailed age model across the PETM was included as a supplement in Hollis et al. (2015). Sediment accumulation rates for Site 277 ranged from ~0.27–8.53 cm/kyr (Fig. 5). Similar to Site 207, a hiatus is identified in the early Eocene at 446.70 mbsf, spanning from lower Zone NP10 to lower Zone NP11 based on the clustering of three bioevents; LO of *Fasciculithus* spp., FO of *T. orthostylus* and FO of *S. radians*. SARs from 54.17 to 53.70 Ma were 3.15 cm/kyr (446.71–431.89 mbsf), somewhat higher than previous estimates of 1.9–2.2 cm/kyr within the Paleogene at Site 277 (Shipboard Scientific Party, 1975). Hollis et al. (1997) documented a much lower rate of sedimentation of 0.56 cm/kyr across a similar interval; however, their rate was calculated from the line of best fit in their age-depth plot, which excluded three potential hiatuses through the interval. The dotted line shown in Fig. 5 of their publication is a closer fit with the age-depth plot shown in this study. The updated age model in Hollis et al. (2015) shows a long hiatus associated with the truncation of the PETM carbon isotope excursion. That age model ignored the LO of *Fasciculithus* (considering it potentially reworked) and instead used the LO of the foraminifera *Subbotina veloscoensis* and a single occurrence of *Discoaster diastypus* for the line of correlation above the PETM. Here we interpret a shorter hiatus associated with the PETM and a longer one that removes much of upper NP10. SARs from 55.76 to 55.64 Ma were 8.53 cm/kyr (456.95–446.71 mbsf).

At the onset of the EECO there was a change to a lower SAR (0.28 cm/kyr) that continued through much of the EECO (53.7–50.5 Ma; 431.89–423.07 mbsf). SARs above this interval of low accumulation were higher for the remainder of the EECO and into Zone NP14 (1.32 cm/kyr) from 50.5 to 46.47 Ma (423.07–369.79 mbsf) A second hiatus is

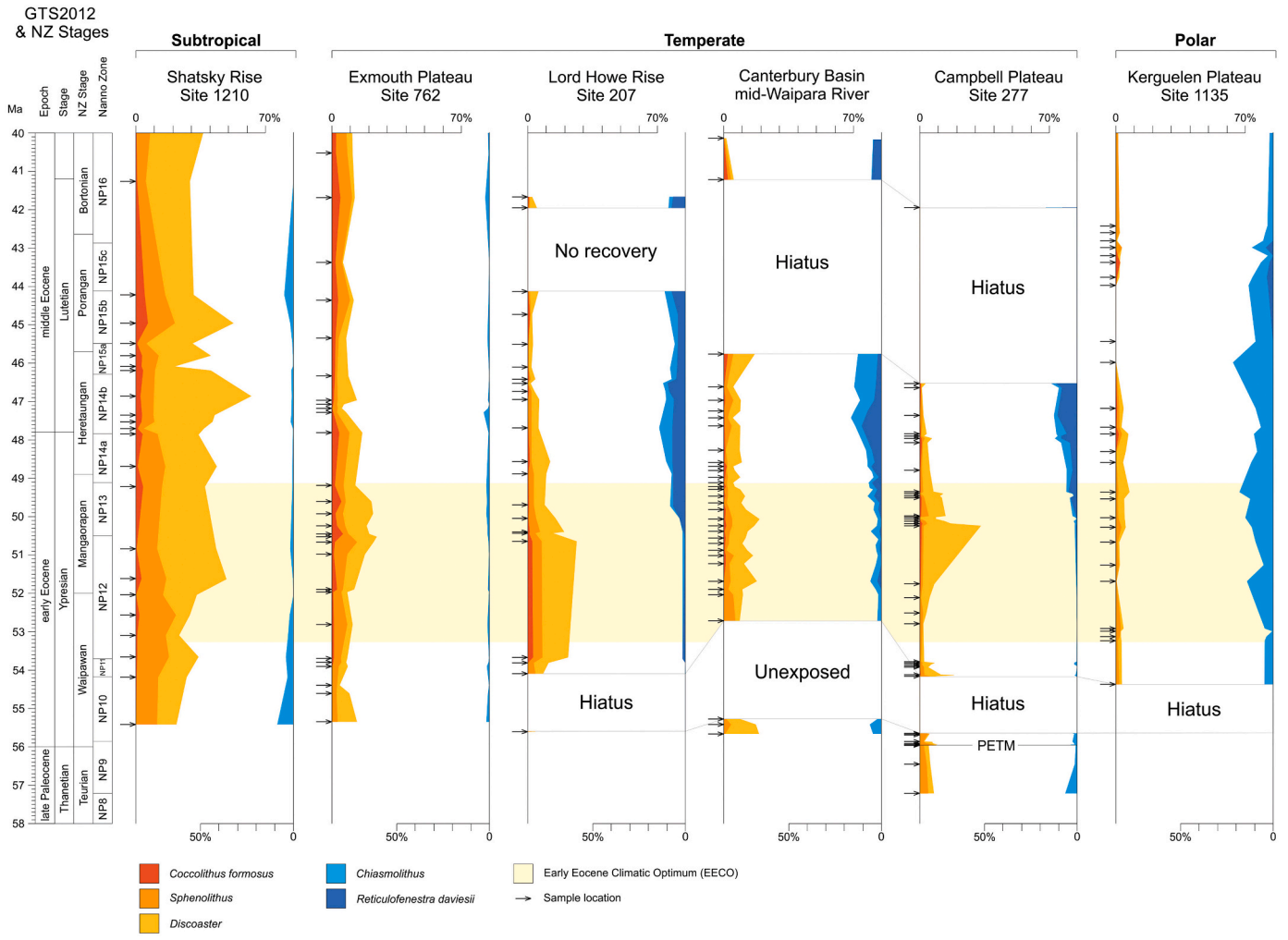

Fig. 6. Relative abundance of key nannofossil warm- and cool-water taxa and genera from selected sites. Data for Shatsky Rise, Exmouth Plateau and Kerguelen Plateau are taken from Schneider et al. (2011) and recalibrated to Gradstein et al. (2012). Yellow shading represents the early Eocene Climatic Optimum (EECO) derived from Hollis et al. (2019) and is tied to the orbitally tuned $\delta^{18}O$ record for Site 1209 (Westerhold et al., 2018).

recognized in the middle Eocene at 369.79 mbsf and includes part of Zone NP14 through basal Zone NP16. This is based on the absences of *N. fulgens* and *P. gigas*, which mark the bases of Subzones NP15a and NP15b, respectively.

6. Discussion

6.1. Nannofossil bioevents in the Southwest Pacific

6.1.1. Rhomboaster lineage

No specimens of *Rhomboaster* were found at either Site 207 or 277, which is consistent with previous observations that this lineage is rare in the SW Pacific region (e.g., Edwards, 1971; Edwards and Perch-Nielsen, 1974; Hollis et al., 2015; Shepherd and Kulhanek, 2016). For Site 207, only one sample was examined that might be the correct age to contain *Rhomboaster*, so it is not surprising that this group was not found at this site. On the other hand, a number of samples were examined across the 34-cm thick PETM from Site 277. Calcareous nannofossils through that section are common and moderately preserved. Deformed discoasters, some similar to *Discoaster nobilis* (sensu Raffi and De Bernardi, 2008) are present, whereas *Rhomboaster*, *Discoaster araneus*, and *Discoaster anortios* are absent (Hollis et al., 2015). Although the carbon isotope excursion is truncated at Site 277, indicating that some of the PETM is missing, the consistent presence of *Fasciculithus* spp. above the PETM interval indicates that this part of the section is still within Zone NP10 (i.e., should contain *R. bramlettei*) and markers for the base of Zone NP11 first appear ~10.5 m above the top of the truncated PETM (Appendix 2). Seven samples with moderately preserved nannofossil assemblages examined over that 10.5 m interval contain neither *R. bramlettei*, nor *T. contortus*. The absence of this group across the PETM is consistent with observations from other PETM sections in the New Zealand region, including Tawanui (Crouch et al., 2003) and Mead Stream (Hollis et al., 2005a). On the other hand, *R. bramlettei* and *R. cuspis* are found in the lowermost Eocene of the mid-Waipara River section in Canterbury Basin (Shepherd and Kulhanek, 2016). This ambiguity makes identifying the Zone NP9/NP10 boundary in the SW Pacific difficult using calcareous nannofossils as its absence might be ecological. Alternate bioevents that can be used to identify lower NP10 include the base of common *Campylosphaera eodela* (55.81 Ma) and the top of *Fasciculithus* spp. (55.64 Ma).

6.1.2. Co-occurrence of Tribrachiatus orthostylus and Sphenolithus radians

At Sites 207 and 277, the FO of *T. orthostylus*, an upper Zone NP10 event (54.37 Ma), co-occurs with *S. radians*, which is a secondary marker for the base of Zone NP11 (54.17 Ma) (Backman, 1986; Agnini et al., 2007a). Since there is only a small age difference between the evolution of these taxa (200 kyr), it is possible that sampling resolution impacted our ability to detect a difference. This is possible at Site 207, where there is a 1.8 m sampling gap between the sample in which the taxa co-occur and the next sample below, although this would equate to only ~100 kyr based on the SAR of ~1.83 cm/kyr through that interval. At Site 277, the

sample gap is only 40 cm, which equates to ~13 kyr based on the SAR of ~3.15 cm/kyr for this interval.

In the Marlborough region (South Island, New Zealand), the FO of *S. radians* was noted in Zone NP12 at Mead Stream (Hollis et al., 2005a); however, nannofossil preservation is very poor at this site. Other sections from Marlborough, including Muzzle and Bluff Streams, also have poor nannofossil preservation in lower Eocene strata. At Bluff Stream, one sample of eight examined from Zone NP11 contains a few specimens of *S. radians*, whereas at Muzzle Stream, *S. radians* was not identified (Hollis et al., 2005b). Poor preservation at these three sites makes it difficult to determine if the FO of *T. orthostylus* and *S. radians* was coeval. However, there is consistency in the co-occurrence of these two species across DSDP Sites 207 and 277 and onshore mid-Waipara River, Canterbury Basin (Shepherd and Kulhanek, 2016; Crouch et al., 2020), which suggests that these two events may have occurred at approximately the same time in the SW Pacific.

6.1.3. Evolution of Reticulofenestra

The FO of the genus *Reticulofenestra* in the equatorial Pacific is dated at 50.5 Ma, coeval with the NP12/NP13 zone boundary (Expedition 320/321 Scientists, 2010; Gradstein et al., 2012). In other low and mid-latitude sites the origination of *Reticulofenestra* has been documented at about the same time (e.g., Aubry, 1998; Bown et al., 2004; Agnini et al., 2006; Schneider et al., 2011). However, Schneider et al. (2011) demonstrated that this origination is diachronous, and that the genus first evolved earlier (~52 Ma; lower NP12) in the high-latitude Southern Ocean at Maud Rise and the Kerguelen Plateau. In the New Zealand region, the evolutionary first occurrence of this genus occurs even lower in the section (in Zone NP11), as previously documented from DSDP Site 277 and mid-Waipara River (Hollis et al., 2015; Shepherd and Kulhanek, 2016) and here extended to Lord Howe Rise at Site 207 (this study).

6.1.4. Reticulofenestra umbilicus

At Sites 207 and 277, it is difficult to identify the base of Zone NP16 due to the absence of the marker taxon *Blackites gladius* (which, as noted previously, ranges above the base of Zone NP16 when present [Wei and Wise Jr., 1989]) and sporadic occurrence of the secondary marker, *Nannotetrina fulgens* (LO = 42.87 Ma). In this study, we have used the FO of *Reticulofenestra umbilicus* > 14 μm (41.94 Ma) to indicate lower Zone NP16; however, at Site 207 this taxon first occurs in low numbers at the same depth as the LO of *P. gigas* (44.12 Ma) and below the LO of *Nannotetrina* spp.; a similar pattern is seen at DSDP Sites 206 and 208 (Appendix 2). At IODP Site U1508, Reinga Basin (Sutherland et al., 2019), the FO of *R. umbilicus* > 14 μm also occurs before the LO of *Nannotetrina* spp.; this pattern at the Lord Howe Rise region sites could be attributed to reworking of *Nannotetrina*. However, *R. umbilicus* > 14 μm also overlaps with *P. gigas*, which is restricted to Subzone NP15b. Therefore, *R. umbilicus* > 14 μm may evolve earlier in the southern mid- to high latitude SW Pacific region, making its FO unreliable for identifying lower Zone NP16. Agnini et al. (2014) noted this issue and therefore use the base common *R. umbilicus* > 14 μm to define the base of Zone CNE13, which corresponds to lower Zone NP16. Applying their concept of base common (=continuous and hopefully relatively common occurrence) may provide better results in the SW Pacific region, although more data over more continuous sections is needed to test this.

6.2. Regional hiatuses

The lowermost Eocene hiatus identified at both Sites 207 and 277 (Fig. 6) encompasses upper Zone NP10 (~55.64–54.17 Ma; this corresponds to all of Zone CNE2) and is based on the juxtaposition of the LO of *Fasciculithus* spp. (55.64 Ma) and FOs of *T. orthostylus* (54.37 Ma) and *S. radians* (54.17 Ma). The scarcity of members of the *Rhomboaster* lineage in this region make it difficult to accurately determine the duration of the hiatus as it could also encompass lowermost NP10 (Zone CNE1), as well as some of NP11/lower CNE3. While sampling resolution could make it appear that these events all occur at about the same position in the cores, we find that unlikely, especially for Site 277. At Site 207, there is a 1.8 m sampling gap between the sample that contains the LO of *Fasciculithus* spp. and the sample in which *S. radians* and *T. orthostylus* first co-occur, so it is possible that sedimentation rates were just extremely low (<0.12 cm/kyr) across that interval. At Site 277, there is only a 40 cm sampling gap, providing much stronger evidence for an unconformity in upper NP10. Another possibility is that *Fasciculithus* is reworked into younger sediment at both sites. This is difficult to tell at Site 207 due to the sparse number of samples examined. At Site 277, fasciculiths in side view are consistently identified in samples above the PETM to 446.92 mbsf, with the next sample at 446.50 mbsf containing *T. orthostylus* and *S. radians*. Two samples above that contain possible fasciculiths in end view, but no side views were observed to allow for confident identification. Additionally, there is a distinct assemblage change between the samples above and below the hiatus at Site 277, with a shift from an assemblage with *Prinsius* spp. and common *Toweius pertusus* to an assemblage dominated by other forms of *Toweius*. The sample at 446.50 mbsf also includes the first occurrences of *Jakubowskia leoniae* and *Discoaster kuepperi*, with the latter already relatively common.

Identification of this lowermost Eocene hiatus agrees with Edwards (1973) who noted an unconformity at DSDP Site 207 at ~285 mbsf. Edwards (1973) also identified this hiatus at DSDP Sites 206 and 208 and suggested it was a regional unconformity associated with the Paleocene/Eocene boundary. Shipboard Scientific Party (1975) proposed that this regional unconformity may be present at Site 277. Expedition 371 scientists also reported an early Eocene hiatus of at least 2 Myr duration (spanning Zones NP9 to NP12) at Site U1509, located on the western margin of the New Caledonia Trough (Sutherland et al., 2019).

A major hiatus spanning middle Eocene to Oligocene is present on Lord Howe Rise and in the New Caledonia Trough. This regional hiatus was originally identified in DSDP Legs 21 (Burns et al., 1973) and 90 (Kennett et al., 1986) and was attributed to oceanographic circulation changes resulting from expansion of ice on Antarctica and initiation of the Antarctic Circumpolar Current (ACC) (Kennett and von der Borch, 1986). However, recent drilling during IODP Expedition 371 related the hiatuses with vertical motion and plate deformation resulting from subduction initiation (Sutherland et al., 2019). The length of the hiatus is greater in the New Caledonia Trough (Site 206) than at Lord Howe Rise (Site 208). At Site 206, sediments below the unconformity are late middle Eocene in age (~38–39 Ma) and are overlain by sediments of middle early Oligocene age (~30–31.35 Ma). Thus, the hiatus is 6.65–9 Myr in duration. Sites drilled in the New Caledonia Trough during Expedition 371 also record shorter hiatuses than those drilled on Lord Howe Rise. Site U1507 (northern New Caledonia Trough) had no missing section across the Eocene–Oligocene section, whereas Sites U1509 (southern New Caledonia Trough) and U1508 (Reinga Basin) record hiatuses of ~3 Myr (middle Eocene) and ~ 6 Myr (middle Eocene to Oligocene), respectively (Sutherland et al., 2019). At Site 208 on northern Lord Howe Rise, sediments below the unconformity are middle Eocene in age (41.6–42.6 Ma) and are overlain by middle lower Oligocene sediments that are slightly younger than those at Site 206, yielding a duration for the hiatus of 11.6–13.0 Myr. This hiatus is significantly longer on southern Lord Howe Rise (Site 207), with sediments overlying the unconformity of middle Miocene age (~15.1–14.5 Ma), yielding a hiatus duration of ~25 Myr. Site U1506, located between Sites 208 and 207, has a hiatus of ~20 Myr spanning from the middle Eocene to the latest Oligocene. Site U1510, which is located northwest of Site 207, also has a long hiatus (~17.5 My) spanning from the late Eocene to the early Miocene (Sutherland et al., 2019). Sediments overlying the hiatus at Site U1510 are similar in age to those overlying the hiatus at Site 207.

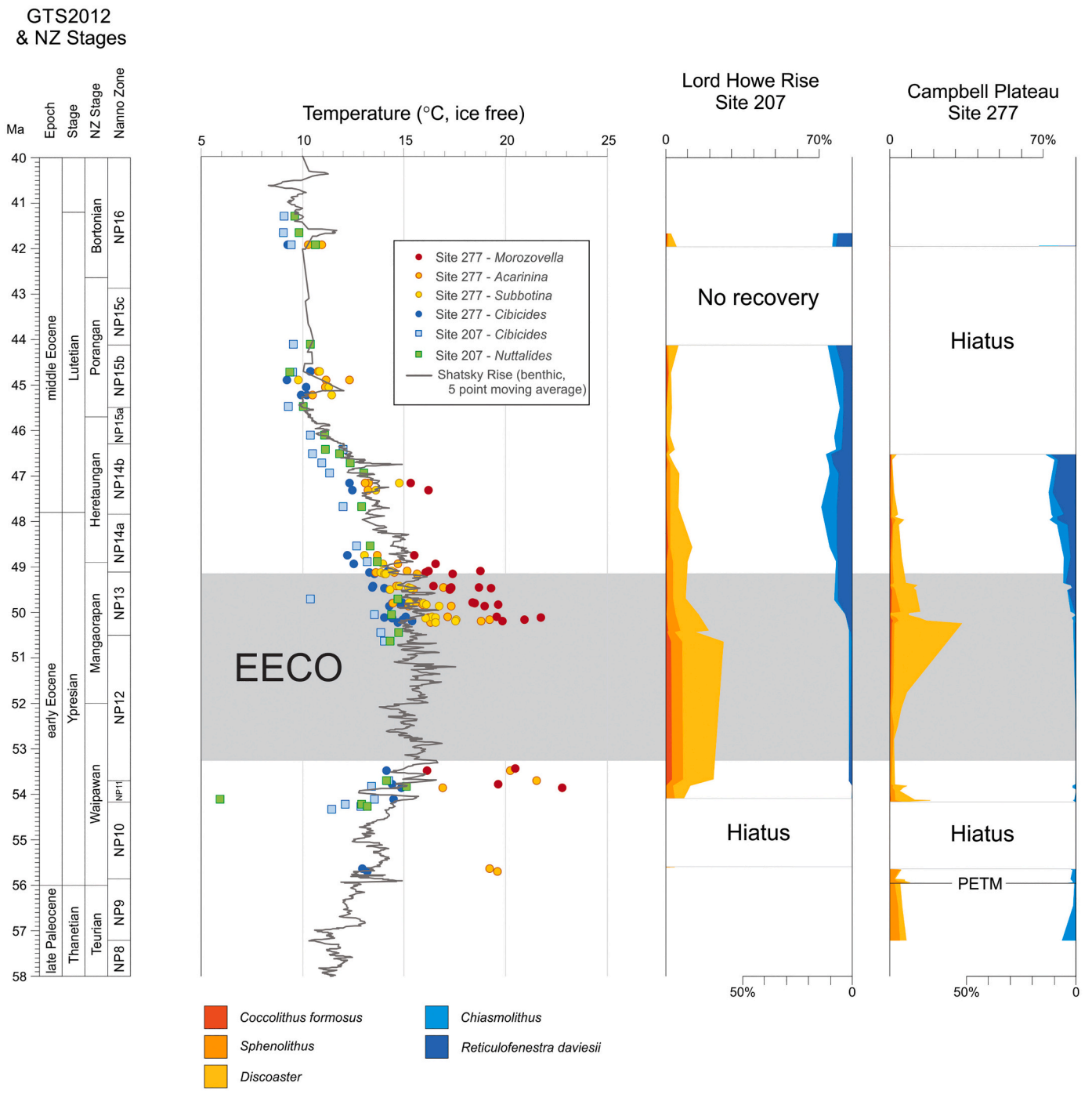

Fig. 7. Sea temperature estimates derived from foraminiferal $\delta^{18}O$ from DSDP Sites 207 and 277 and from the following Shatsky Rise sites: 56–45 Ma, ODP Site 1209 (Westerhold et al., 2018); 45–40 Ma, DSDP Site 577 and ODP Sites 1209 and 1218 (Cramer et al., 2011). To facilitate direct comparison with $\delta^{18}O$ values, a uniform ice-free temperature equation with no latitudinal correction has been applied. The duration of the EECO is derived from Hollis et al. (2019) and is tied to the orbitally tuned $\delta^{18}O$ record for Site 1209 (Westerhold et al., 2018). Relative abundance of key nannofossil warm- and cool-water taxa and genera from Sites 207 and 277 are shown for comparison.

6.3. Early–middle Eocene paleoenvironment

Interpretation of assemblage changes in the early Eocene is complicated by an interval of non-deposition in the earliest Eocene (much of Zone NP10), and lower SAR in the late early Eocene (much of Zone NP12). Additionally, for DSDP Sites 207 and 277 there is low temporal resolution from the available samples through the interval leading into the EECO (Figs. 6 and 7). At both sites, an increase in warm-water taxa occurs prior to the onset of the EECO. At Site 207 it is difficult to determine if this increased abundance is sustained through the initiation of the EECO or whether it corresponds with an earlier hyperthermal event. The upper part of the EECO is recorded by peak numbers of warm-water taxa (~50.7–50.3 Ma), followed by an increase in cool-water taxa from 49 Ma. The interval corresponding to the peak warmth of the EECO is represented by very low rates of deposition at both sites (Figs. 4 and 5).

There is very good agreement between benthic $\delta^{18}O$ records for Sites 207 and 277 and the high-resolution record for Shatsky Rise IODP Site

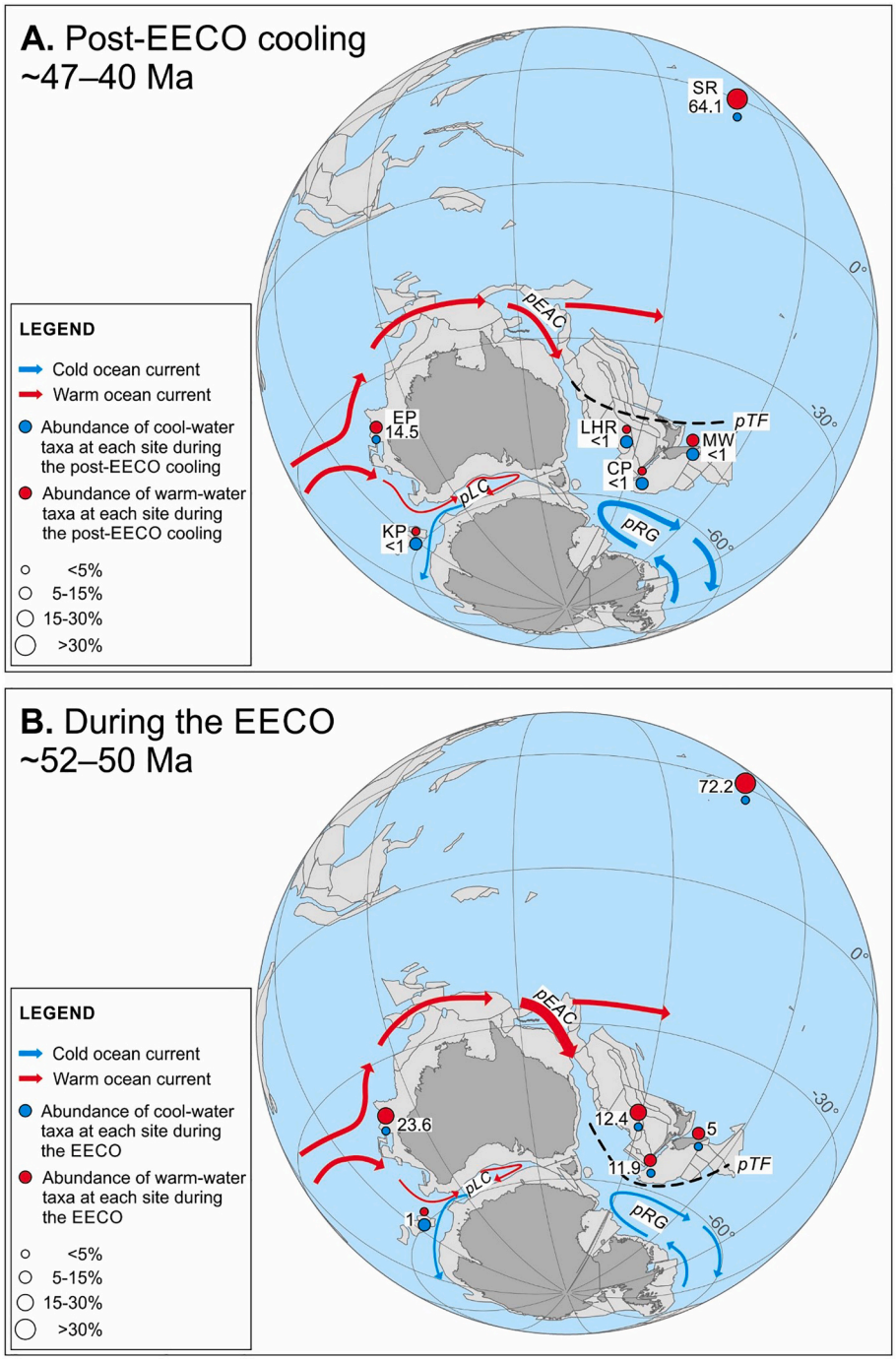

Fig. 8. Paleogeographic reconstructions for sites in the southern middle to high latitudes in the early to middle Eocene. (A) and (B) Ratio of warm- to cool-water taxa at each site. (C) and (D) Number of warm-water taxa at each site. Data for Shatsky Rise (SR), Exmouth Plateau (EP) and Kerguelen Plateau (KP) are from Schneider et al. (2011). Data for mid-Waipara River (MW) are from Crouch et al. (2020). Values are taken as the average over each time interval. Paleogeographic reconstructions are based on the absolute reference frame of Torsvik et al. (2012). pEAC = proto-East Australian Current; pTF = proto-Tasman Front; pRG = proto-Ross Gyre; pLC = proto-Leeuwin Current. LHR = Lord Howe Rise, CP = Campbell Plateau.

1209 (Westerhold et al., 2018; Fig. 7). Despite Sites 207 and 277 lacking a complete record of the EECO, both sites record a warming trend leading up to the EECO followed by progressive cooling from the upper part of the EECO to ~45 Ma, although the warming trend is of shorter duration at Site 277. As at Shatsky Rise, temperatures are relatively stable from 45 to 41 Ma although there are large gaps in the record due to hiatuses and poor core recovery. Calcareous nannofossil assemblages exhibit a similar trend, except that the increase in the abundance of cool-water assemblages stabilizes earlier at both sites, around ~48 Ma.

Planktic foraminifera tests at Site 277 are recrystallized and, therefore, their $\delta^{18}O$ values are thought to suffer from a cool bias (Sexton et al., 2006; Hollis et al., 2015, 2019). With modest recrystallization, temperature gradients between surface and thermocline dwelling taxa may still be evident although damped to some degree (Pearson et al., 2001; Zachos et al., 2002). A significant temperature gradient of 5–8 °C between the near-surface dwelling genera *Morozovella* and *Acarinina* and benthic genus *Cibicides* in the early Eocene indicates that the planktic $\delta^{18}O$ still preserves part of the original temperature signal and thus records modest thermal stratification (Fig. 7). A weak offset of 2–3 °C is also evident between these surface-dwelling taxa and the thermocline genus *Subbotina*. Maximum SST estimates of ~20–23 °C for *Morozovella* within the EECO are significantly lower than the median value of 30 °C for the same genus and interval at Site 277 based on Mg/Ca ratios (Hines et al., 2017; Hollis et al., 2019), a proxy that has been found to be less affected by recrystallization (Sexton et al., 2006; Edgar et al., 2015). Above the EECO and through the middle Eocene, a weakening of the

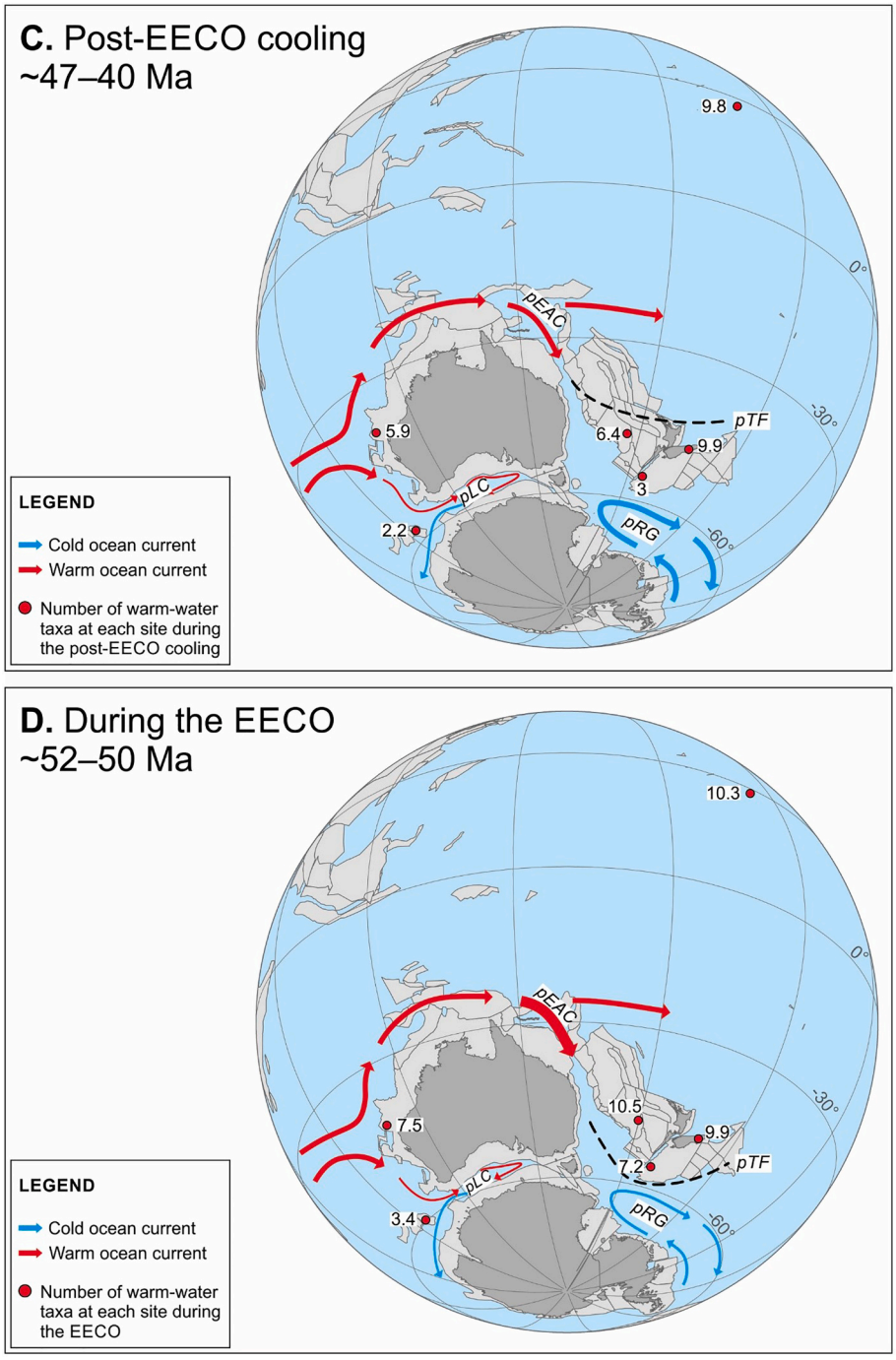

Fig. 8. (*continued*).

temperature gradient between benthic and planktic foraminifera may signal surface water cooling and a reduction in thermal gradients (greater vertical mixing) but also may be due to a greater degree of recrystallization, perhaps associated with the cooler water temperatures.

6.4. Regional comparison

Early to middle Eocene warm-water nannofossil assemblages from DSDP Sites 207 and 277 are most similar to those documented from other temperate sites (Exmouth Plateau and Canterbury Basin), rather than assemblages from subtropical (Shatsky Rise) or subpolar (Kerguelen Plateau) sites (Fig. 6). During the EECO, warm-water assemblages reach a maximum of 27% at Site 207 and 33% at Site 277. This is comparable with mid-Waipara River, Canterbury Basin, New Zealand (Shepherd, 2017; Crouch et al., 2020), and ODP Site 762, Exmouth Plateau (Schneider et al., 2011), where warm-water taxa comprise up to 19% and 24%, respectively, in the EECO. At subpolar ODP Site 1135, Kerguelen Plateau, warm-water assemblages reach a maximum of 7% of the total assemblage during the EECO and at the subtropical ODP Site 1210, Shatsky Rise, they account for up to 49% of the total assemblage (Schneider et al., 2011).

Conversely, cool-water taxa at Sites 207 and 277 have a much lower abundance through the EECO, forming no more than 8% and 12% of the total assemblage, respectively (Figs. 6 and 7). This is comparable with mid-Waipara River at 7% (Shepherd, 2017; Crouch et al., 2020) and Site 762 at 1.7% (Schneider et al., 2011). Cold-water assemblages at high-latitude Site 1135 still constitute up to 18% of the assemblage during

the EECO (Schneider et al., 2011). At Sites 207 and 277 the abundance of cool-water taxa starts to increase towards the termination of the EECO (Figs. 6 and 7).

The early Eocene nannofossil assemblages examined in this study are indicative of warm temperate conditions for the SW Pacific, rather than tropical conditions inferred from geochemical proxies (Bijl et al., 2009; Hollis et al., 2009, 2012, 2015; Creech et al., 2010; Hines et al., 2017). Although Sites 207 and 277 show an increase in warm-water assemblages through the EECO, abundance is not as high as that recorded at low-latitudes (Schneider et al., 2011). The generally low abundance of warm-water taxa at these SW Pacific sites and relatively short episodes of warm-water incursions are difficult to reconcile with the tropical conditions inferred from geochemical proxies for the entire EECO.

6.5. Early–middle Eocene surface-water circulation in the SW Pacific

Nannofossil data from this study are broadly in agreement with inferences drawn from previous studies (e.g., Jenkins, 1993; Nelson and Cooke, 2001; Kennett and Exon, 2004; Sijp et al., 2011). Calculation of the ratio between warm- and cool-water taxa at each site identifies a clear pattern of warm and cool assemblages through the early to middle Eocene. During the early Eocene (~50–56 Ma) assemblages from the SW Pacific sites consisted predominantly of warm-water taxa, suggesting that a warm-water mass extended to ~55°S paleolatitude at this time. Although SW Pacific nannofossil assemblages appear to have been influenced by warmer surface waters, it is unlikely that temperatures reached tropical levels, as the ratio of warm- to cool-water taxa is still well below that of low-latitude sites (e.g., Shatsky Rise; Fig. 8B), even though diversity of warm-water taxa is comparable at both latitudes (Fig. 8D). Instead, it appears that the boundary between warm subtropical and temperate waters, here referred to as the proto-Tasman Front (proto-TF), migrated southward in response to enhanced poleward heat transport.

During the middle Eocene (47–40 Ma), cool-water taxa became more abundant in SW Pacific nannofossil assemblages and diversity also decreased, indicating a shift towards cooler conditions (Figs. 8A and C). It is likely that the proto-TF shifted north of ~45°S paleolatitude and this was accompanied by an intensification of a proto-Ross Gyre (proto-RG; Fig. 8A and C). This is in agreement with Nelson and Cooke (2001), who suggested that cooling in the middle Eocene was likely accompanied by a return of the transition zone between warm subtropical and temperate waters to ~50°S paleolatitude. This pattern of frontal movement during cooler intervals is also consistent with Quaternary studies, which indicate northerly migration of the Subtropical Front to around 45–46°S during cool phases such as Marine Isotope Stages 3 and 4 (Sikes et al., 2009).

Diversity and abundance of warm-water taxa was greatest at Site 207, implying that a proto-EAC exerted greater influence at this site throughout the EECO. Warm-water was transported to Site 277 as the proto-EAC intensified; however, the relatively short-lived influx of warm-water taxa suggests that this warmth was not sustained for the entirety of the EECO. The peak abundance of warm-water taxa was lower in the Canterbury Basin (mid-Waipara River; Crouch et al., 2020) than at Sites 207 and 277 during the EECO (Fig. 6), suggesting that the warming of surface waters associated with the expansion of the proto-EAC was not as influential in the Canterbury region of New Zealand as in the west (Fig. 8B).

7. Conclusions

Calcareous nannofossil assemblages from legacy DSDP sites in the SW Pacific provide evidence of significant warming of mid-latitude surface waters during the early Eocene. Variations in the relative abundance of warm- and cool-water taxa are consistent with the trends seen in geochemical-based temperature proxy records. The highest abundance of warm-water taxa at both DSDP Sites 207 and 277 coincides with the EECO, which is in agreement with global evidence for this interval being a sustained period of prolonged global warmth in the Cenozoic.

However, early Eocene nannofossil assemblages at Sites 207 and 277 indicate warm temperate conditions, rather than the tropical conditions inferred for the SW Pacific from geochemical proxies (Bijl et al., 2009; Hollis et al., 2009, 2012, 2015; Creech et al., 2010; Hines et al., 2017; Crouch et al., 2020). This signal from nannofossil assemblages is in agreement with radiolarian assemblages in the SW Pacific, which were dominated by cosmopolitan taxa and only low numbers of low-latitude, tropical-subtropical taxa during the early Eocene (Hollis et al., 2014, 2020). Marine dinoflagellate assemblages from mid-Waipara River, Canterbury Basin, also exhibit a similar trend to that observed in SW Pacific nannofossil assemblages (Crouch et al., 2020).

Benthic foraminiferal $\delta^{18}O$ values from DSDP Sites 207 and 277 exhibit similar trends to the nannofossil assemblages, recording a warming interval leading up to the EECO, followed by a progressive cooling in the upper part of the EECO to ~45 Ma. Despite the likely effects of recrystallization of foraminiferal tests at Site 277, SSTs indicated by planktic foraminifera agree with warm temperate conditions rather than tropical conditions. Our work on these legacy sites provides a valuable platform for future studies on new cores retrieved during recent IODP expeditions in the SW Pacific, Expedition 371 (Lord Howe Rise) and Expedition 378 (Campbell Plateau).

Supplementary data to this article can be found online at https://doi.org/10.1016/j.marmicro.2021.101992.

Declaration of Competing Interest

The authors declare that they have no known competing financial interests or personal relationships that could have appeared to influence the work reported in this paper.

Acknowledgements

CLS, CJH, KMP, HEGM and CPS acknowledge support from the New Zealand Marsden Fund and the GNS Science Strategic Science Investment Fund. We thank Dyke Andreason and Colin Carney (UCSC SIL) for technical support. Samples from DSDP Sites 206, 207, 208 and 277 were provided by the International Ocean Discovery Program.

References

Agnini, C., Muttoni, G., Kent, D.V., Rio, D., 2006. Eocene biostratigraphy and magnetic stratigraphy from Possagno, Italy: the calcareous nannofossil response to climate variability. Earth Planet. Sci. Lett. 241, 815–830.

Agnini, C., Fornaciari, E., Raffi, I., Rio, D., Rohl, U., Westerhold, T., 2007a. High-resolution nannofossil biochronology of middle Paleocene to early Eocene at ODP Site 1262: implications for calcareous nannoplankton evolution. Mar. Micropaleontol. 64, 215–218. https://doi.org/10.1016/j.marmicro.2007.05.003.

Agnini, C., Fornaciari, E., Rio, D., Tateo, F., Backman, J., Giusberti, L., 2007b. Responses of calcareous nannofossil assemblages, mineralogy and geochemistry to the environmental perturbations across the Paleocene/Eocene boundary in the Venetian Pre-Alps. Mar. Micropaleontol. 63 (1–2), 19–38. https://doi.org/10.1016/j.marmicro.2006.10.002.

Agnini, C., Fornaciari, E., Raffi, I., Catanzariti, R., Pälike, H., Backman, J., Rio, D., 2014. Biozonation and biochronology of Paleogene calcareous nannofossils from low and middle latitudes. Newsl. Stratigr. 47 (2), 131–181.

Anagnostou, E., John, E.H., Edgar, K.M., Foster, G., Ridgwell, A., Inglis, G.N., Pancost, R. D., Lunt, D.J., Pearson, P.N., 2016. Changing atmospheric CO_2 concentration was the primary driver of early Cenozoic climate. Nature. https://doi.org/10.1038/nautre17423.

Aubry, M.P., 1991. Sequence stratigraphy: eustasy or tectonic imprint? J. Geophys. Res. 96 (B4), 6641–6679. https://doi.org/10.1029/90JB01204.

Aubry, M.P., 1992. Late Paleogene calcareous nannoplankton evolution: a tale of climatic deterioration. In: Prothero, D.R., Berggren, W.A. (Eds.), Eocene–Oligocene Climate and Biotic Evolution. Princeton University Press, Princeton, NJ, pp. 272–309.

Aubry, M.P., 1998. Early Paleogene calcareous nannoplankton evolution: a tale of climatic amelioration. In: Aubry, M.P., Lucas, S., et al. (Eds.), Late Paleocene–Early Eocene Climatic and Biotic Events in the Marine and Terrestrial Records. Columbia University Press, New York, pp. 158–203.

Aubry, M.-P., Ouda, K., Dupuis, C., Berggren, W.A., Van Couvering, J.A., the Members of the Working Group on the Paleocene/Eocene Boundary, 2007. The global standard stratotype-section and point (GSSP) for the base of the Eocene Series in the Dababiya section (Egypt). Episodes 30 (4), 271–286.

Backman, J., 1986. Late Paleocene to middle Eocene calcareous nannofossil biochronology from the Shatsky Rise, Walvis Ridge and Italy. Palaeogeogr. Palaeoclimatol. Palaeoecol. 57, 43–59.

Bijl, P.K., Schouten, S., Sluijs, A., Reichart, G.-J., Zachos, J.C., Brinkhuis, H., 2009. Early Palaeogene temperature evolution of the southwest Pacific Ocean. Nature 461 (7265), 776–779. https://doi.org/10.1038/nature08399.

Bijl, P.K., Pross, J., Warnaar, J., Stickley, C.E., Huber, M., Guerstein, R., Houben, A.J.P., Sluijs, A., Visscher, H., Brinkhuis, H., 2011. Environmental forcings of Paleogene Southern Ocean dinoflagellate biogeography. Paleoceanography 26, PA1202. https://doi.org/10.1029/2009PA001905.

Bijl, P.K., Bendle, J.A., Bohaty, S.M., Pross, J., Schouten, S., Tauxe, L., Stickley, C.E., McKay, R.M., Röhl, U., Olney, M., Sluijs, A., Escutia, C., Brinkhuis, H., Expedition 318 Scientists, 2013. Eocene cooling linked to early flow across the Tasmanian Gateway. PNAS 110 (24), 9645–9650. https://doi.org/10.1073/pnas.1220872110.

Bown, P.R., 1998. Calcareous Nannofossil Biostratigraphy. Kluwer Academic Publishers, London, p. 315.

Bown, P.R., 2005. Paleogene calcareous nannofossils from the Kilwa and Lind areas of coastal Tanzania (Tanzania Drilling Project 2003–4). J. Nannoplankton Res. 27 (1), 21–95.

Bown, P.R., Newsam, C., 2017. Calcareous nannofossils from the Eocene North Atlantic Ocean (IODP Expedition 342 Sites U1403–1411). J. Nannoplankton Res. 37 (1), 26–60.

Bown, P.R., Young, J.R., 1998. Techniques. In: Bown, P.R. (Ed.), Calcareous Nannofossil Biostratigraphy. Kluwer Academic Publishers, London, pp. 16–28.

Bown, P.R., Lees, J.A., Young, J.R., 2004. Calcareous nannoplankton evolution and diversity through time. In: Thierstein, H.R., Young, J.R. (Eds.), Coccolithophores: From Molecular Processes to Global Impact. Springer-Verlag, Berlin, pp. 481–508.

Bralower, T.J., 2002. Evidence of surface water oligotrophy during the Paleocene-Eocene thermal maximum: nannofossil assemblage data from Ocean Drilling Program Site 690, Maud Rise, Weddell Sea. Paleoceanography 17 (2), 13–1-NaN-13–12. https://doi.org/10.1029/2001pa000662.

Bukry, D., 1973. Coccolith and silicoflagellate biostratigraphy, Tasman Sea and southwest Pacific Ocean, Deep Sea Drilling Project Leg 21. In: Burns, R.E., Andrews, J.E. (Eds.), Initial Reports of the Deep Sea Drilling Project (Vol. 21). US Government Printing Office, Washington, DC, pp. 885–893.

Burns, R.E., Andrews, J.E., Van der Lingen, G.J., Churkin, M., Galehouse, J.S., Packham, G.H., Davies, T.A., Kennett, J.P., Dumitrica, P., Edwards, A.R., Von Herzen, R.P., 1973. Initial Reports of the Deep Sea Drilling Project. (Vol. 21). US Government Printing Office, Washington DC, pp. 197–212.

Cappelli, C., Bown, P.R., De Riu, M., Agnini, C., 2020. Middle Eocene large coccolithaceans: biostratigraphic implications and paleoclimatic clues. Mar. Micropaleontol. 154 https://doi.org/10.1016/j.marmicro.2019.101812.

Cooper, R.A., 2004. The New Zealand geological timescale: Institute of Geological and Nuclear Sciences Monograph 22, p. 284.

Cramer, B.S., Miller, K.G., Barrett, P.J., Wright, J.D., 2011. Late Cretaceous–Neogene trends in deep ocean temperature and continental ice volume: reconciling records of benthic foraminiferal geochemistry (δ18O and Mg/Ca) with sea level history. J. Geophys. Res.: Oceans 116, C12023. https://doi.org/10.1029/2011jc007255.

Creech, J.B., Baker, J.A., Hollis, C.J., Morgans, H.E.G., Smith, E.G.C., 2010. Eocene sea temperatures for the mid-latitude southwest Pacific from Mg/Ca ratios in planktonic and benthic foraminifera. Earth Planet. Sci. Lett. 299 (3–4), 483–495. https://doi.org/10.1016/j.epsl.2010.09.039.

Crouch, E.M., Dickens, G.R., Brinkhuis, H., Aubry, M.-P., Hollis, C.J., Rogers, K.M., Visscher, H., 2003. The *Apectodinium* acme and terrestrial discharge during the Paleocene–Eocene thermal maximum: new palynological, geochemical and calcareous nannoplankton observations at Tawanui, New Zealand. Palaeogeogr. Palaeoclimatol. Palaeoecol. 194, 387–403.

Crouch, E.M., Shepherd, C.L., Morgans, H.E.G., Naafs, B.D.A., Dallanave, E., Phillips, A., Hollis, C.J., Pancost, R.D., 2020. Climatic and environmental changes across the Early Eocene Climatic Optimum at mid-Waipara River, Canterbury Basin, New Zealand. Earth-Sci. Rev. https://doi.org/10.1016/j.earscirev.2019.102961.

Dallanave, E., Agnini, C., Bachtadse, V., Muttoni, G., Crampton, J.S., Strong, C.P., Hines, B.R., Hollis, C.J., Slotnick, B.S., 2015. Early to middle Eocene magneto-biochronology of the southwest Pacific Ocean and climate influence on sedimentation: Insights from the Mead Stream section, New Zealand. Geol. Soc. Am. Bull. 127, 643–660.

Dallanave, E., Bachtadse, V., Crouch, E.M., Tauxe, L., Shepherd, C.L., Morgans, H.E.G., Hollis, C.J., Hines, B.R., Sugisaki, S., 2016. Constraining early to middle Eocene climate evolution of the southwest Pacific and Southern Ocean. Earth Planet. Sci. Lett. 433, 380–392. https://doi.org/10.1016/j.epsl.2015.11.010.

de Hornibrook, N.B., Brazier, R.C., Strong, C.P., 1989. Manual of New Zealand Permian to Pleistocene foraminiferal biostratigraphy. New Zeal. Geol. Surv. Paleontol. Bull. 56, 175.

Dunkley Jones, T., Bown, P.R., Pearson, P.N., Wade, B.S., Coxall, H.K., Lear, C.H., 2008. Major shifts in calcareous phytoplankton assemblages through the Eocene-Oligocene transition of Tanzania and their implications for low-latitude primary production. Paleoceanography 23, PA4204. https://doi.org/10.1029/2008PA001640.

Dunkley Jones, T., Bown, P.R., Pearson, P.N., 2009. Exceptionally well preserved upper Eocene to lower Oligocene calcareous nannofossils (Prymnesiophyceae) from the Oande Formation (Kilwa Group), Tanzania. J. Syst. Palaeontol. 7 (4), 359–411.

Edgar, K.M., Anagnostou, E., Pearson, P.N., Foster, G.L., 2015. Assessing the impact of diagenesis on δ11B, δ13C, δ18O, Sr/Ca and B/Ca values in fossil planktic foraminiferal calcite. Geochim. Cosmochim. Acta 166, 189–209.

Edwards, A.R., 1971. A calcareous nannoplankton zonation of the New Zealand Paleogene. In: Paper presented at the Proceedings of the Second Planktonic Conference, Roma.

Edwards, A.R., 1973. Southwest Pacific regional unconformities encountered during Leg 21. In: Burns, R.E., Andrews, J.E., et al. (Eds.), Initial Reports of the Deep Sea Drilling Project (Vol. 21). US Government Printing Office, Washington, DC, pp. 701–720.

Edwards, A.R., Perch-Nielsen, K., 1974. Calcareous nannofossils from the southern Southwest Pacific, Deep Sea Drilling Project, Leg 29. In: Kennett, J.P., Houtz, R.E., et al. (Eds.), Initial Reports of the Deep Sea Drilling Project, Vol. 29. Washington (U. S. Government Printing Office), pp. 469–539.

Expedition 320/321 Scientists, 2010. Methods. In: Pälike, H., Lyle, M., et al. (Eds.), Proceedings of the Integrated Ocean Drilling Program, 320/321. Integrated Ocean Drilling Program Management International, Tokyo.

Fioroni, C., Villa, G., Persico, D., Jovane, L., 2015. Middle Eocene-lower Oligocene calcareous nannofossil biostratigraphy and paleoceanographic implications from Site 711 (equatorial Indian Ocean). Mar. Micropaleontol. 118, 50–62.

Gibbs, S.J., Bralower, T.J., Bown, P.R., Zachos, J.C., Bybell, L.M., 2006. Shelf and open-ocean calcareous phytoplankton assemblages across the Paleocene–Eocene thermal maximum. Earth Planet. Sci. Lett. 295, 583–592.

Gradstein, F.M., Ogg, J.G., Schmitz, M., Ogg, G., 2012. The Geologic Time Scale 2012: Elsevier, p. 1176.

Haq, B.U., Lohmann, G.P., 1976. Early Cenozoic calcareous nannoplankton biogeography of the Atlantic Ocean. Mar. Micropaleontol. 1, 119–194. https://doi.org/10.1016/0377-8398(76)90008-6.

Haq, B.U., Premoli-Silva, I., Lohmann, G.P., 1977. Calcareous plankton paleobiogeographic evidence for major climatic fluctuations in the early Cenozoic Atlantic Ocean. J. Geophys. Res. 82 (27), 3861–3876.

Hines, B.R., Hollis, C.J., Atkins, C.B., Baker, J.A., Morgans, H.E.G., Strong, C.P., 2017. Reduction of oceanic temperature gradients in the early Eocene Southwest Pacific Ocean. Palaeogeogr. Palaeoclimatol. Palaeoecol. 475, 41–54.

Hollis, C.J., Waghorn, D.B., Strong, C.P., Crouch, E.M., 1997. Integrated Paleogene Biostratigraphy of DSDP site 277 (Leg 29): Foraminifera, Calcareous Nannofossils, Radiolaria, and Palynomorphs. Institute of Geological & Nuclear Sciences science report 97/07, p. 87.

Hollis, C.J., Dickens, G.R., Field, B.D., Jones, C.M., Strong, C.P., 2005a. The Paleocene–Eocene transition at Mead Stream, New Zealand: a southern Pacific record of early Cenozoic global change. Palaeo. 215, 313–343.

Hollis, C.J., Field, B.D., Jones, C.M., Strong, C.P., Wilson, G.J., Dickens, G.R., 2005b. Biostratigraphy and carbon isotope stratigraphy of uppermost Cretaceous-lower Cenozoic Muzzle Group in middle Clarence valley, New Zealand. J. R. Soc. New Zeal. 35 (3), 345–383.

Hollis, C.J., Handley, L., Crouch, E.M., Morgans, H.E.G., Baker, J.A., Creech, J., Collins, K.S., Gibbs, S.J., Huber, M., Schouten, S., Zachos, J.C., Pancost, R.D., 2009. Tropical sea temperatures in the high-latitude South Pacific during the Eocene. Geology 37 (2), 99–102. https://doi.org/10.1130/G25200A.

Hollis, C.J., Taylor, K.W.R., Handley, L., Pancost, R.D., Huber, M., Creech, J.B., Hines, B. R., Crouch, E.M., Morgans, H.E.G., Crampton, J.S., Gibbs, S., Pearson, P.N., Zachos, J.C., 2012. Early Paleogene temperature history of the Southwest Pacific Ocean: reconciling proxies and models. Earth Planet. Sci. Lett. 349–350, 53–66. https://doi.org/10.1016/j.epsl.2012.06.024.

Hollis, C.J., Pascher, K.M., Hines, B.R., Littler, K., Kulhanek, D.K., Strong, C.P., Zachos, J. C., Eggins, S.M., Phillips, A., 2014. Was the early Eocene ocean unbearably warm or are the proxies unbelievably wrong? Rend. Online Soc. Geol. Ital. 31, 109–110.

Hollis, C.J., Hines, B.R., Littler, K., Villasante-Marcos, V., Kulhanek, D.K., Strong, C.P., Zachos, J.C., Eggins, S.M., Northcote, L., Phillips, A., 2015. The Paleocene-Eocene Thermal Maximum at DSDP Site 277, Campbell Plateau, southern Pacific Ocean. Clim. Past 11, 1009–1025. https://doi.org/10.5194/cp-11-1009-2015.

Hollis, C.J., Dunkley Jones, T., Anagnostou, E., Bijl, P., Cramwinckel, M., Edgar, K., et al., 2019. The DeepMIP contribution to PMIP4: methodologies for selection, compilations and analysis of latest Paleocene and early Eocene climate proxy data. Geosci. Model Dev. https://doi.org/10.5194/gmd-2018-309.

Hollis, C.J., Pascher, K.M., Sanfilippo, A., Nishimura, A., Kamikuri, S.-I., Shepherd, C.L., 2020. An Austral radiolarian biozonation for the Paleogene. Stratigraphy 17 (4), 213–278.

Huber, M., Caballero, R., 2011. The early Eocene equable climate problem revisited. Clim. Past 7, 603–633. https://doi.org/10.5194/cp-7-603-2011.

Jenkins, D.G., 1971. New Zealand Cenozoic Planktonic Foraminifera. New Zeal. Geol. Surv. Paleontol. Bull. 42, 278.

Jenkins, D.G., 1993. The evolution of the Cenozoic southern high- and mid-latitude planktonic foraminiferal faunas. In: Kennett, J.P., Warnke, D.A. (Eds.), The Antarctic Paleoenvironment: A Perspective on Global Change, Part 2, Antarctic Research Series, Vol. 60. American Geophysical Union, pp. 175–194.

Kalb, A.L., Bralower, T.J., 2012. Nannoplankton origination events and environmental changes in the late Paleocene and early Eocene. Mar. Micropaleontol. 92–93, 1–15.

Katz, M.E., Katz, D.R., Wright, J.D., Miller, K.G., Pak, D.K., Shackleton, N.J., Thomas, E., 2003. Early Cenozoic benthic foraminiferal isotopes: species reliability and interspecies correction factors. Paleoceanography 18, 1024. https://doi.org/10.1029/2002PA000798.

Kennett, J.P., Exon, N.F., 2004. Paleoceanographic evolution of the Tasmanian Seaway and its climatic implications. In: Exon, N.F., Kennett, J.P., et al. (Eds.), The Cenozoic Southern Ocean: Tectonics, Sedimentation, and Climate Change between Australia and Antarctica. AGU, Washington, DC, pp. 345–367.

Kennett, J.P., von der Borch, C.C., 1986. Southwest Pacific Cenozoic paleoceanography. In: Kennett, J.P., von der Borch, C.C., et al. (Eds.), Init. Repts. DSDP, 90. Washington DC (U.S. Government Printing Office), pp. 1493–1517.

Kennett, J.P., von der Borch, C.C., Baker, P.A., Barton, C.E., Boersma, A., Caulet, J.P., Dudley, W.C., Gardner, J.V., Jenkins, D.G., Lohman, W.H., Martini, E., Merrill, R.B., Morin, R., Nelson, C.S., Robert, C., Srinivasan, M.S., Stein, R., Takeuchi, A., 1986. Initial Reports of the Deep Sea Drilling Project, Vol. 90. US Government Printing Office, Washington DC.

Kim, S.-T., O'Neil, J.R., 1997. Equilibrium and nonequilibrium oxygen isotope effects in synthetic carbonates. Geochim. Cosmochim. Acta 61, 3461–3475.

Kulhanek, D.K., Crouch, C.M., Tayler, M.J.S., Hollis, C.J., 2015. Paleocene calcareous nannofossils from East Coast, New Zealand: biostratigraphy and paleoecology. J. Nannoplankton Res. 35, 155–176.

Lohman, W.H., 1986. Calcareous nannoplankton biostratigraphy of the southern Coral Sea, Tasman Sea, and Southwestern Pacific Ocean, Deep Sea Drilling Project Leg 90: Neogene and Quaternary. In: Kennett, J.P., von der Borch, C.C., et al. (Eds.), Init. Repts. DSDP, 90. Washington DC (U.S. Government Printing Office), pp. 763–793.

Lunt, D.J., Dunkley Jones, T., Heinemann, M., Huber, M., LeGrande, A., Winguth, A., Loptson, C., Marotzke, J., Roberts, C.D., Tindall, J., Valdes, P., Winguth, C., 2012. A model-data comparison for a multi-model ensemble of early Eocene atmosphere-ocean simulations: EoMIP. Clim. Past 8, 1717–1736.

Lunt, D.J., Bragg, F., Chan, W.L., Hutchinson, D.K., Ladant, J.B., Morozova, P., Niezgodzki, I., Steinig, S., Zhang, Z., Zhu, J., Abe-Ouchi, A., Anagnostou, E., de Boer, A.M., Coxall, H.K., Donnadieu, Y., Foster, G., Inglis, G.N., Knorr, G., Langebroek, P.M., Lear, C.H., Lohmann, G., Poulsen, C.J., Sepulchre, P., Tierney, J. E., Valdes, P.J., Volodin, E.M., Dunkley Jones, T., Hollis, C.J., Huber, M., Otto-Bliesner, B.L., 2021. DeepMIP: model intercomparison of early Eocene climatic optimum (EECO) large-scale climate features and comparison with proxy data. Clim. Past 17 (1), 203–227.

Martini, E., 1971. Standard Tertiary and Quaternary calcareous nannoplankton zonation. In: Paper presented at the Proceedings of the Second Planktonic Conference, Roma.

Matthews, K.J., Maloney, K.T., Zahirovic, S., Williams, S.E., Seton, M., Müller, R.D., 2016. Global plate boundary evolution and kinematics since the late Paleozoic. Glob. Planet. Chang. 146, 226–250.

McIntyre, A., Bé, A.W.H., 1967. Modern Coccolithophoridae of the Atlantic Ocean - I. Placoliths and cyrtoliths. Deep-Sea Res. 14, 561–597.

Nelson, C.S., Cooke, P.J., 2001. History of oceanic front development in the New Zealand sector of the Southern Ocean during the Cenozoic—A synthesis. New Zeal. J. Geol. Geophys. 44 (4), 535–553. https://doi.org/10.1080/00288306.2001.9514954.

Okada, H., Honjo, S., 1973. The distribution of oceanic coccolithophorids in the Pacific. Deep-Sea Res. 20, 355–374.

Pancost, R.D., Taylor, K.W.R., Inglis, G.N., Kennedy, E.M., Handley, L., Hollis, C.J., Crouch, E.M., Pross, J., Huber, M., Schouten, S., Pearson, P.N., Morgans, H.E.G., Raine, J.I., 2013. Early Paleogene evolution of terrestrial climate in the SW Pacific, Southern New Zealand. Geochem. Geophys. Geosyst. 14 (12), 5413–5429. https://doi.org/10.1002/2013GC004935.

Pascher, K.M., 2017. Paleobiogeography of Eocene Radiolarians in the Southwest Pacific. Unpublished PhD thesis. Victoria University of Wellington, New Zealand, p. 323.

Pearson, P.N., Ditchfield, P.W., Singano, J., Harcourt-Brown, K.G., Nicholas, C.J., Olsson, R.K., Shackleton, N.J., Hall, M.A., 2001. Warm tropical sea surface temperatures in the Late Cretaceous and Eocene epochs. Nature 413 (6855), 481–487.

Pearson, P.N., Olsson, R.K., Huber, B.T., Hemleben, C., Berggren, W.A. (Eds.), 2006. Atlas of Eocene Planktonic Foraminifera. Cushman Foundation for Foraminiferal Reasearch Special Publication, 41, p. 513.

Perch-Nielsen, K., 1985. Cenozoic calcareous nannofossils. In: Bolli, H., Perch-Nielsen, K., et al. (Eds.), Plankton Stratigraphy. Cambridge University Press, New York, pp. 427–554.

Persico, D., Villa, G., 2004. Eocene–Oligocene calcareous nannofossils from Maud Rise and Kerguelen Plateau (Antarctica): paleoecological and paleoceanographic implications. Mar. Micropaleontol. 52 (1–4), 153–179. https://doi.org/10.1016/j.marmicro.2004.05.002.

Raine, J.I., Beu, A.G., Boyes, A.F., Campbell, H.J., Cooper, R.A., Crampton, J.S., Crundwell, M.P., Hollis, C.J., Morgans, H.E.G., 2015. Revised calibration of the New Zealand Geological Timescale: NZGT2015/1 GNS Science Report 2012/39, p. 53.

Raffi, I., De Bernardi, B., 2008. Response of calcareous nannofossils to the Paleocene–Eocene Thermal Maximum: Observations on composition, preservation and calcification in sediments from ODP Site 1263 (Walvis Ridge – SW Atlantic). Mar. Micropal. 69, 119–138.

Röhl, U., Westerhold, T., Bralower, T.J., Zachos, J.C., 2007. On the duration of the Paleocene-Eocene thermal maximum (PETM). Geochem. Geophys. Geosyst. 8 (12), Q12002 https://doi.org/10.1029/2007GC001784.

Schneider, L.J., Bralower, T.J., Kump, L.R., 2011. Response of nannoplankton to early Eocene ocean destratification. Palaeoceanogr. Palaeoclimatol. Palaeoecol. 310, 152–162.

Self-Trail, J.M., Powars, D.S., Watkins, D.K., Wandless, G.A., 2012. Calcareous nannofossil assemblage changes across the Paleocene-Eocene Thermal Maximum: evidence from a shelf setting. Mar. Micropaleontol. 92–93, 61–80. https://doi.org/10.1016/j.marmicro.2012.05.003.

Sexton, P.F., Wilson, P.A., Pearson, P.N., 2006. Microstructural and geochemical perspectives on planktic foraminiferal preservation: "Glassy" versus "Frosty". Geochem. Geophys. Geosyst. 7, Q12p19.

Shackleton, N.J., Kennett, J.P., 1975. Paleotemperature history of the Cenozoic and the initiation of Antarctic glaciation: oxygen and carbon isoptope analyses in DSDP Sites 277, 279, and 281. In: Kennett, J.P., Houtz, R.E., et al. (Eds.), Initial Reports of the Deep Sea Drilling Project, Vol. 29. Washington, DC: US Government Printing Office, pp. 743–755.

Shamrock, J.L., Watkins, D.K., 2012. Eocene calcareous nannofossil biostratigraphy and community structure from Exmouth Plateau, Eastern Indian Ocean (ODP Site 762). Stratigraphy 9 (1), 54.

Shepherd, C.L., 2017. Early to Middle Eocene Calcareous Nannofossils of the SW Pacific: Paleobiogeography and Paleoclimate. Unpublished PhD thesis. Victoria University of Wellington, p. 171.

Shepherd, C.L., Kulhanek, D.K., 2016. Eocene nannofossil biostratigraphy of the mid-Waipara River section, Canterbury Basin, New Zealand. J. Nannoplankton Res. 36 (1), 33–59.

Shipboard Scientific Party, 1975. Site 277. In: Kennett, J.P., Houtz, R.E., et al. (Eds.), Initial Reports of the Deep Sea Drilling Project, Vol. 29. US Government Printing Office, Washington DC, pp. 45–120.

Sijp, W., England, M.H., Huber, M., 2011. Effect of the deepening of the Tasman Gateway on the global ocean. Paleoceanography 26 (1–18), 2011. https://doi.org/10.1029/2011PA002143.

Sikes, E.L., Howard, W.R., Samson, C.R., Mahan, T.S., Robertson, L.G., Volkman, J.K., 2009. Southern Ocean seasonal temperature and Subtropical Front movement on the South Tasman Rise in the late Quaternary. Paleoceanography 46, 1–13. https://doi.org/10.1029/2008PA001659.

Slotnick, B.S., Dickens, G.R., Hollis, C.J., Crampton, J.S., Strong, C.P., Phillips, A., 2015. The onset of the Early Eocene Climatic Optimum at Branch Stream, Clarence River valley, New Zealand. New Zeal. J. Geol. Geophys. 58, 262–280.

Sutherland, R., 1999. Basement geology and tectonic development of the greater New Zealand region: an interpretation from Regional magnetic data. Tectonophysics 308 (3), 341–362. https://doi.org/10.1016/S0040-1951(99)00108-0.

Sutherland, R., Dickens, G.R., Blum, P., Expedition 371 Scientists, 2019. Tasman Frontier subduction initiation and Paleogene climate. In: Proceedings of the International Ocean Discovery Program, 371: College Station, TX (International Ocean Discovery Program) doi:10.14379/iodp.proc.371.2019.

Taylor, K.W.R., Huber, M., Hollis, C.J., Hernandez-Sanchez, M.T., Pancost, R.D., 2013. *Re*-evaluating modern and Palaeogene GDGT distributions: implications for SST reconstructions. Glob. Planet. Chang. 108, 158–174.

Taylor, K.W.R., Willumsen, P.S., Hollis, C.J., Pancost, R.D., 2018. South Pacific evidence for the long-term climate impact of the Cretaceous/Paleogene boundary event. Earth-Sci. Rev. 179, 287–302.

Tjalsma, R.C., Lohmann, G.P., 1983. Paleocene–Eocene bathyal and abyssal benthic foraminifera from the Atlantic Ocean. Micropaleontol. Specl. Publ. 4, 1–90.

Torsvik, T.H., Van der Voo, R., Preeden, U., Mac Niocaill, C., Steinberger, B., Doubrovine, P.V., van Hinsbergen, D.J.J., Domeier, M., Gaina, C., Tohver, E., Meert, J.G., McCausland, P.J.A., Cocks, L.R.M., 2012. Phanerozoic polar wander, palaeogeography and dynamics. Earth Sci. Rev. 114, 325–368.

van Morkhoven, F.P.C.M., Berggren, W.A., Edwards, A.S., 1986. Cenozoic cosmopolitan deep-water benthic foraminfera. In: Bulletin des Centres de Recherches Exploration-Production Elf-Aquitaine Memoire, Vol. 11, p. 421.

Villa, G., Persico, D., 2006. Late Oligocene climatic changes: evidence from calcareous nannofossils at Kerguelen Plateau Site 748 (Southern Ocean). Palaeogeogr. Palaeoclimatol. Palaeoecol. 231 (1–2), 110–119. https://doi.org/10.1016/j.palaeo.2005.07.028.

Villa, G., Fioroni, C., Pea, L., Bohaty, S., Persico, D., 2008. Middle Eocene–late Oligocene climate variability: Calcareous nannofossil response at Kerguelen Plateau, Site 748. Mar. Micropaleontol. 69 (2), 173–192. https://doi.org/10.1016/j.marmicro.2008.07.006.

Villa, G., Fioroni, C., Persico, D., Roberts, A.P., Florindo, F., 2014. Middle Eocene to Late Oligocene Antarctic glaciation/deglaciation and Southern Ocean productivity. Paleoceanography 29, 223–237. https://doi.org/10.1002/2013PA002518.

Wei, W., 2004. Opening of the Australia-Antarctica Gateway as dated by nannofossils. Mar. Micropaleontol. 52, 133–152. https://doi.org/10.1016/j.marmicro.2004.04.008.

Wei, W., Wise, S.W., 1990. Biogeographic gradients of middle Eocene–Oligocene calcareous nannoplankton in the South Atlantic Ocean. Palaeogeogr. Palaeoclimatol. Palaeoecol. 79 (1–2), 29–61. https://doi.org/10.1016/0031-0182(90)90104-F.

Wei, W., Wise Jr., S.W., 1989. Paleogene calcareous nannofossil magnetobiochronology: results from South Atlantic DSDP Site 516. Mar. Micropaleontol. 14, 119–152.

Wei, W., Villa, G., Wise, S.W., 1992. Paleoceanographic implications of Eocene–Oligocene calcareous nannofossils from Sites 711 and 748 in the Indian Ocean. In: Wise Jr., S.W., Schlich, R., et al. (Eds.), Proceedings of the Ocean Drilling Program, Scientific Results, 120. College Station, TX, pp. 979–999.

Westerhold, T., Röhl, U., Donner, B., Zachos, J.C., 2018. Global extent of the Early Eocene hyperthermal events – A new Pacific benthic foraminiferal isotope record from Shatsky Rise (ODP site 1209). Paleoceanogr. Paleoclimatol. 33, 626–642. https://doi.org/10.1029/2017PA003306.

Zachos, J.C., Arthur, M.A., Bralower, T.J., Spero, H.J., 2002. Tropical temperatures in greenhouse episodes. Nature 419, 897–898. https://doi.org/10.1038/419897b.

Zachos, J.C., Dickens, G.R., Zeebe, R.E., 2008. An early Cenozoic perspective on greenhouse warming and carbon-cycle dynamics. Nature 45, 279–283.